TURUN
YLIOPISTO
UNIVERSITY
OF TURKU

CONTROLLED DECORATION OF MOLECULAR SPHERICAL NUCLEIC ACIDS

Vijay Gulumkar

TURUN YLIOPISTON JULKAISUJA – ANNALES UNIVERSITATIS TURKUENSIS
SARJA – SER. AI OSA – TOM. 676 | ASTRONOMICA – CHEMICA – PHYSICA – MATHEMATICA | TURKU 2022

TURUN
YLIOPISTO
UNIVERSITY
OF TURKU

CONTROLLED DECORATION OF MOLECULAR SPHERICAL NUCLEIC ACIDS

Vijay Gulumkar

TURUN YLIOPISTON JULKAISUJA – ANNALES UNIVERSITATIS TURKUENSIS
SARJA – SER. AI OSA – TOM. 676 | ASTRONOMICA - CHEMICA - PHYSICA – MATHEMATICA | TURKU 2022

University of Turku

Faculty of Science
Department of Chemistry
Chemistry
Doctoral programme in Exact Sciences

Supervised by

Professor, Pasi Virta
Department of Chemistry
University of Turku
Turku, Finland

Associate Professor, Tuomas Lönnberg
Department of Chemistry
University of Turku
Turku, Finland

Reviewed by

Professor, Steven Dowdy
Department of Cellular and Molecular Medicine, University of California, San Diego, School of Medicine, USA

Professor, Mikko Oivanen
Department of Chemistry
University of Helsinki
Helsinki, Finland

Opponent

Professor, Roger Strömberg
Department of Biosciences and Nutrition
Karolinska Institutet
Stockholm, Sweden

ISBN 978-951-29-9025-2 (PRINT)
ISBN 978-951-29-9026-9 (PDF)
ISSN 0082-7002 (Print)
ISSN 2343-3175 (Online)
Painosalama, Turku, Finland 2022

Dedicated to My Dear Grandmother

UNIVERSITY OF TURKU
Faculty of Science
Department of Chemistry
Chemistry
VIJAY GULUMKAR: Controlled Decoration of Molecular Spherical Nucleic Acids
Doctoral Dissertation, 114 pp.
Doctoral Programme in Exact Sciences
October 2022

ABSTRACT

Research on therapeutically effective oligonucleotides (antisense oligonucleotides, ASOs and small interfering RNAs, siRNAs) has grown rapidly during the last decades. Oligonucleotide (ON) therapeutics are nowadays an effective drug modality for the treatment of many diseases. However, oligonucleotides therapeutic potential is still limited by known issues; e.g., premature elimination via renal clearance, unfavourable bio-distribution, and poor cellular uptake, which considerably restrict systemic delivery of ONs to target cells. To address some of these issues, covalent conjugation of oligonucleotides with ligands, that have affinity for a specific cell type, may enhance cell uptake and targeted delivery of ONs. Spherical nucleic acids (SNAs) provide an attractive alternative formulation option for ONs, because they may overcome some of the restrictions of traditional nucleic acids.

This thesis describes syntheses of molecularly defined C_{60}-based SNAs, including new core units and controlled decoration approaches. A controlled monofunctionalization of molecular SNAs on an azide-functionalized [C_{60}]fullerene has been developed. This methodology allows controlled functionalization of one oligonucleotide arm on the SNAs, for example with labels or other conjugate groups. Glycocluster-oligonucleotide conjugates were prepared, hybridized with complementary strands of a C_{60}-based SNA and cellular uptake of these glyco-decorated SNAs with PC3 prostate cancer cells were preliminary studied. A bifunctional C_{60}-core was prepared, that can be selectively one-pot functionalized by two successive pericyclic click reactions (i.e., inverse electron-demand Diels-Alder cycloaddition, iEDDA and strain promoted azide-alkyne cycloaddition, SPAAC). By using this core unit, hetero-antennary SNAs (including glycoballs and glyco-peptide structures) have been assembled. This synthetic strategy may find interesting applications as novel delivery vehicles, in which tissue specific ligands and drug payloads may be loaded on the same SNA in an orthogonal way.

KEYWORDS: fullerene, oligonucleotide, spherical nucleic acid, glycocluster, oligonucleotide conjugate, tergeted delivery

TURUN YLIOPISTO
Matemaattis-luonnontieteellinen tiedekunta
Kemian laitos
kemia
VIJAY GULUMKAR: Controlled Decoration of Molecular Spherical Nucleic Acids
Väitöskirja, 114 s.
Eksaktien tieteiden tohtoriohjelma
lokakuu 2022

TIIVISTELMÄ

Kiinnostus oligonukleotidien mahdollisuuksiin lääkeaineina on kasvanut nopeasti kahden viime vuosikymmenen aikana. Nykyään niitä voidaankin jo pitää varteenotettava lääkemodaliteettina useisiin sairauksiin. Niiden käyttö on kuitenkin yhä rajoittunut, mikä johtuu oligonukleotidien heikoista lääkekuljetin ominaisuuksista systeemisessä annostelussa. Näitä ovat esimerkiksi heikko soluun otto, epäsuotuisa biologinen jakautuminen ja ennenaikainen munuaissuodatus, jotka rajoittavat oligonukleotidien pääsyä kohdekudokseen ja –soluun. Näitä ongelmia pystytään ratkomaan osin, kun oligonukleotideihin liitetään kovalenttisesti solu- tai kudoshakuisia ligandeja, mutta tämäkin mahdollisuus rajoittuu tiettyihin erityistapauksiin. Pallonukleiinihapot ovat mielenkiintoinen mahdollisuus oligonukleotidien lääkekuljetinominaisuuksien tehostamiseksi. Niissä oligonukelotidit rakennetaan tiheäksi kuoreksi sopivan runkorakenteen ympärille. Nämä kontrolloidusti rakennetut nanopartikkelit voivat tehostaa ligandivälitteistä kudos- ja soluspesifisyyttä.

Tämä väitöskirjatutkimus keskittyy molekulaarisesti määriteltyjen ja kontrolloidusti pintarakenteeltaan muokattujen C_{60}-fullereeniin pohjautuvien pallonukleiinihappojen synteesistrategioihin. Tutkimuksessa optimoitiin menetelmä, jossa pallonukleiinihapporakenteita pystyään monofunktionalisoimaan helposti, selektiivisesti ja hyvällä saannolla. Tämä on tärkeä menetelmä, kun halutaan minimoida leiman vaikutusta tarkasteltavan pallonukleiinihapon biologisten ominaisuuksien tarkastelussa. Samaa menetelmää voidaan hyödyntää myös pallonukleiinihappojen konjugoimiseen muihin lääkekuljetinmolekyyleihin; esimerkiksi vasta-aineisiin tai aptameereihin. Tutkimuksessa syntetisoitiin myös ortogonaalisesti muokattu fullereenirakenneyksikkö, joka mahdollistaa uudenlaisten heterobifunktionaalisten pallonukleiinihappojen valmistamisen yhdessä reaktioastiassa. Tutkimuksen kolmantena kohteena olivat sokerikuorrutetut pallonukleiinihapot, joiden kokoamisessa hyödynnettiin kaksoiskierteen muodostumista. Kyseisissä rakenteissa ligandi-soluvuorovaikutuksen odotetaan tehostuvan. Rakenteilla tehtiin alustavia solukokeita.

ASIASANAT: Fullereeni, oligonukleotidi, oligonukleotidikonjugaatti, pallonukleiinihappo, glykoklusteri, lääkeainekuljetus

Table of Contents

Abbreviations

Ab	antibody
Ac	acetyl
AFM	atomic force microscopy
ASO	antisense oligonucleotide
ASGPR	asialoglycoprotein receptor
BBB	blood-brain barrier
BCN	bicycle[6.1.0]non-4-yn-9-ylmethanol and 2-bicycle[6.1.0]non-4-yn-9-yl
CD	circular dichroism
CE	capillary electrophoresis
COSY	correlation spectroscopy
CPG	controlled pore glass
CT	computed tomography
DBU	1,8-diazabicyclo[5.4.0]undec-7-ene
DBCO	dibenzocyclooctyne
DCA	dichloroacetic acid
CD44	cluster of differentiation 44
DCM	dichloromethane
DIAD	diisopropyl azodicarboxylate
DLS	dynamic light scattering
DMF	*N,N*-dimethylformamide
DMSO	dimethyl sulfoxide
DMPK	dystrophia myotonica protein kinase
DM1	myotonic dystrophy type 1
DNA	deoxyribonucleic acid
dsRNA	double-stranded RNA
DOTA	1,4,7,10-tetraazacyclododecane1,4,7,10-tetraacetic acid
EMA	european medicines agency
ESI-MS	electrospray ionization mass spectrometry
Fab	fragment antigen-binding
FDA	food and drug administration (U. S. A)

Gal	galactose
GalNAc	*N*-acetylgalactosamine
GBM	glioblastoma
Glu	glucose
HMBC	heteronuclear multiple bond correlation
HPLC	high performance liquid chromatography
HSQC	heteronuclear single quantum coherence
iEDDA	inverse electron-demand Diels-Alder cycloaddition
LNA	locked nucleic acid
LNP	lipid nano particle
mAb	monoclonal antibody
Man	mannose
ACN	acetonitrile
mRNA	messenger RNA
MXD3	MAX dimerization protein 3
NMR	nuclear magnetic resonance
NP	nanoparticle
ON	oligonucleotide
PAGE	Polyacrylamide gel electrophoresis
PAMAM	polyamidoamine
PEG	polyethylene glycol
PET	positron emission tomography
PLGA	poly(lactic-co-glycolic acid)
PNA	peptide nucleic acid
PS	phosphorothioate
RISC	RNA-induced silencing complex
RNA	ribonucleic acid
RNAi	RNA interference
RNase	ribonuclease
RP HPLC	reverse phase HPLC
rt	room temperature
SEC-MALS	size exclusion chromatography equipped with a multiple angle light scattering detector
SELEX	systematic evolution of ligands by exponential enrichment
siRNA	small interfering RNA
SNA	spherical nucleic acid
SPAAC	strain promoted azide-alkyne cycloaddition
SSO	splice switching oligonucleotide
TCO	trans-cyclooctene
TFA	trifluoroacetic acid

THF	tetrahydrofuran
T_m	melting temperature
UV	ultraviolet

List of Original Publications

This dissertation is based on the following original publications, which are referred to in the text by their Roman numerals:

I Gulumkar, V., Äärelä, A., Moisio, O., Rahkila, J., Tähtinen, V., Leimu, L., Korsoff, N., Korhonen, H., Poijärvi-Virta, P., Mikkola, S., Nesati, V., Vuorimaa-Laukkanen, E., Viitala, T., Yliperttula, M., Roivainen, A., and Virta, P. Controlled Monofunctionalization of Molecular Spherical Nucleic Acids on a Buckminster Fullerene Core. *Bioconjugate Chem.*, 2021; 32: 1130-1138.

II Tähtinen, V., Gulumkar, V., Maity, S. K., Yliperttula, A-M., Siekkinen, S., Laine, T., Lisitsyna, E., Haapalehto, I., Viitala, T., Vuorimaa-Laukkanen, E., Yliperttula, M., and Virta, P. Assembly of Bleomycin Saccharide-Decorated Spherical Nucleic Acids. *Bioconjugate Chem.*, 2022; 33: 206-218.

III Gulumkar, V., Tähtinen, V., Ali, A., Rahkila, J., Valle-Delgado, J. J., Äärelä, A., Österberg, M., Yliperttula, M., and Virta, P. Synthesis of an Azide- and Tetrazine-Functionalized [60] Fullerene and Its Controlled Decoration with Biomolecules. *ACS Omega*, 2022; 7: 1329-1336.

List of Related Publications

I Jadhav, S., Gulumkar, V., Deshpande, P., Coffey, E. T., Lönnberg, H., and Virta, P. Synthesis of Azide-Modified Chondroitin Sulfate Precursors: Substrates for ‘‘Click’’-Conjugation with Fluorescent Labels and Oligonucleotides. *Bioconjugate Chem.*, 2018; 29: 2382-2393.

1 Introduction

For the past four decades, research on therapeutically relevant nucleic acids (antisense oligonucleotides, ASOs and small interfering RNAs, siRNA) has grown rapidly. Nucleic acid-based agents have become an effective drug modality for the treatment of many diseases. To date 13 oligonucleotide (ON) drugs have been approved by United States Food and Drug Administration (FDA) and European Medicines Agency (EMA), including Fomivirsen (ASO, 1998), Mipomersen (ASO, 2013), Eteplirsen (ASO, 2016), Nusinersen (ASO, 2016), Inotersen (ASO, 2018), Patisiran (siRNA, 2018), Golodirsen (ASO, 2019), Givosiran (siRNA, 2019), Volanesorsen (ASO, 2019), Viltolarsen (ASO, 2020), Lumasiran (siRNA, 2020), Inclisiran (siRNA, 2020) and Casimersen (ASO, 2021).[1] However, ON drugs have the known problems, which are related mainly to their delivery. Intravenously injected ONs are prone to premature elimination via renal clearance, they accumulate to liver cells, which/and are susceptible to enzymatic degradation and show poor cellular uptake. These significantly restrict systemic delivery of ONs to the target cells. Safe and effective delivery of nucleic acid-based therapeutics requires the sophisticated delivery platforms. Some problems may be solved by the covalent conjugation of ONs with ligands that have affinity for a specific cell type. For example, *N*-acetylgalactosamine (GalNAc)-conjugated ONs are used to improve the cell uptake and targeted delivery of ONs to liver hepatocytes via receptor-mediated endocytosis. In addition, variety of nanocarriers such as liposomes, polymeric nanoparticles, micelles and lipid nanoparticles have been utilized. They have shown encouraging results in pre-clinical and clinical trials, indicating that nanoparticle carriers may be the solution for the delivery.[2,3]

Spherical nucleic acids (SNAs) have emerged as an attractive delivery option among the developed nanoparticle-based delivery vehicles.[4,5] SNAs are constructed by densely packed shell of ONs on an appropriate core unit. SNAs three-dimensional structure provides the unique physiochemical and biological properties: they are taken into cells efficiently without any co-carriers through scavenger receptor-mediated endocytosis.[6] They protect ONs against nuclease degradation,[7] and show low immunogenicity and toxicity,[8,9] which can avoid renal clearance, and have

ability to enter blood-tumor barrier.[10] SNAs can function in gene regulation,[4,11–15] drug delivery,[16–20] and immunomodulation agents.[21]

1.1 Therapeutic oligonucleotides

Nucleic acids, deoxyribonucleic acid (DNA) and ribonucleic acid (RNA) are essential elements of life, in which small pieces of the genetic information, called nucleic acids, are connected to each other via sugar phosphate backbone (**Figure 1**). Nucleotides are consisted nucleobases: adenine, cytosine, guanine, thymine (DNA) and uracil (RNA), which are bound via *N*-glycosidic bond either to 2-deoxyribose (DNA), or to ribose (RNA) sugar. The nucleobases contain hydrogen bonding acceptors and donors, which in appropriate shape complementarities and conformational requirements are responsible for specific binding, i.e., Watson-Crick-base pairing, between single strand nucleic acids to form the double helices. DNA stores the genetic information, specific to a single individual of all living forms, and is responsible to transfer this information to next generation of the species. The role of RNA is more diverse, playing important role in various biological processes such as coding, decoding, catalysis, regulation and expression of genes. The information transfers from DNA to the eventual protein formation: in particular, splicing of pre-mature RNA (pre-mRNA) to messenger RNA (mRNA) and the mRNA-specific translation machinery to cognate proteins, and the option to interfere these processes by exogenous single strand ONs and double helical RNAs offers possibilities to the modern ON-based drug design (cf. mechanism of actions in **Figure 3**).

The advantage of this drug modality is that it is not limited to druggability of a disease-causing protein, which may be perceived to the classical small molecular drug design. The proof of concept, in which a protein production could be down-regulated by exposing cells to a short synthetic ON (i.e. ASO) was described for the first time in 1978 by Zamecnik and Stephenson.[22,23] The mechanism of this RNase-H-mediated cleavage of mRNA was discovered one year later. This breakthrough received a wide visibility, gave an impression that we could develop the ON-based drugs for any disease just by rapid rational design that is based on the Watson Crick-base pairing. This was partly true. The initial hopes remained mainly unfulfilled. The fact is that the ONs are negatively charged macromolecules, and they are not "drug-like". They are susceptible to nuclease-mediated degradation, and physicochemical characteristics lead to modest cellular uptake and unfavourable biodistribution.

The first ASO drug Fomivirsen (i.e. Vitravene) was approved by FDA in 1998. Fomivirsen was a 21-mer oligo 2'-deoxyribonucleotide, with a phosphorothioate backbone that increased its stability against nucleases. It was intraocularly administered and used against cytomegalovirus retinitis in immunocompromised patients (primarily AIDS patients). This drug was later withdrawn from use due to

reduced clinical need and the next ASO drug, Mipomersen (i.e. Kynamro, 2013), was approved after fifteen years. Kynamro represented the next generation ASO drugs, being a 20-mer phosphorothioate gapmer of 2'-deoxyribonucleotides and 2'-*O*-methoxyethyl-modified ribonucleotides. Kynamro was used as treatment for hypercholesterolemia, and it was administrated subcutaneously. This drug was later rejected by EMA for safety reasons. After this somewhat sluggish and disappointing period, a clear new advent of ON therapeutics was seen. This included breakthroughs, in which different mechanisms of action were utilized: Nusinersen (Spinraza) was the first FDA-approved (2016) splice switching oligonucleotide (SSO). It was 2´-*O*-methoxyethyl (MOE) modified phosphorothioate, 18 nucleotides in length, administrated intrathecally to spinal cord, and used for treatment of spinal muscular atrophy (SMA). It restored the function of survival motor neuron 2 (SMN2) mRNA regenerating the cognate protein SMN production. It shown to be a highly effective therapy for both infantile- and later-onset types of SMA.[24,25]

Patisiran (Onpattro) was the first FDA-approved (2018) siRNA. It consisted of double helical naked RNA, both strands 21 nucleotides in length. 5-Methyl cytosine and uracil nucleobases used to avoid immunogenicity and antisense strand contained the typical two thymidine overhang in the 5'-terminus. Because of the naked RNA structure, Patisiran was susceptible to nuclease-mediated cleavage. This was prevented by the lipid nanoparticle (LNP) formulation. This formulation also facilitated Patisiran's delivery to liver and cellular uptake to hepatocytes.

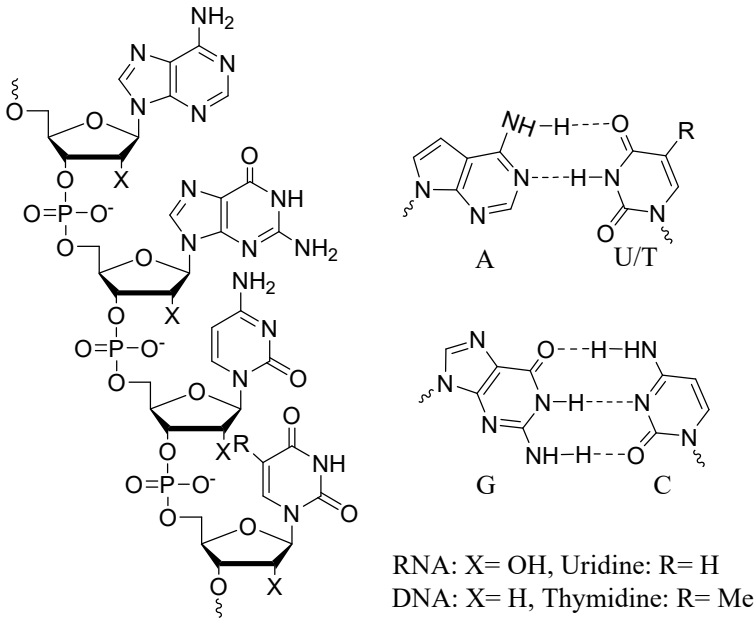

Figure 1. The structure of DNA and RNA and Watson-crick base-pairing.

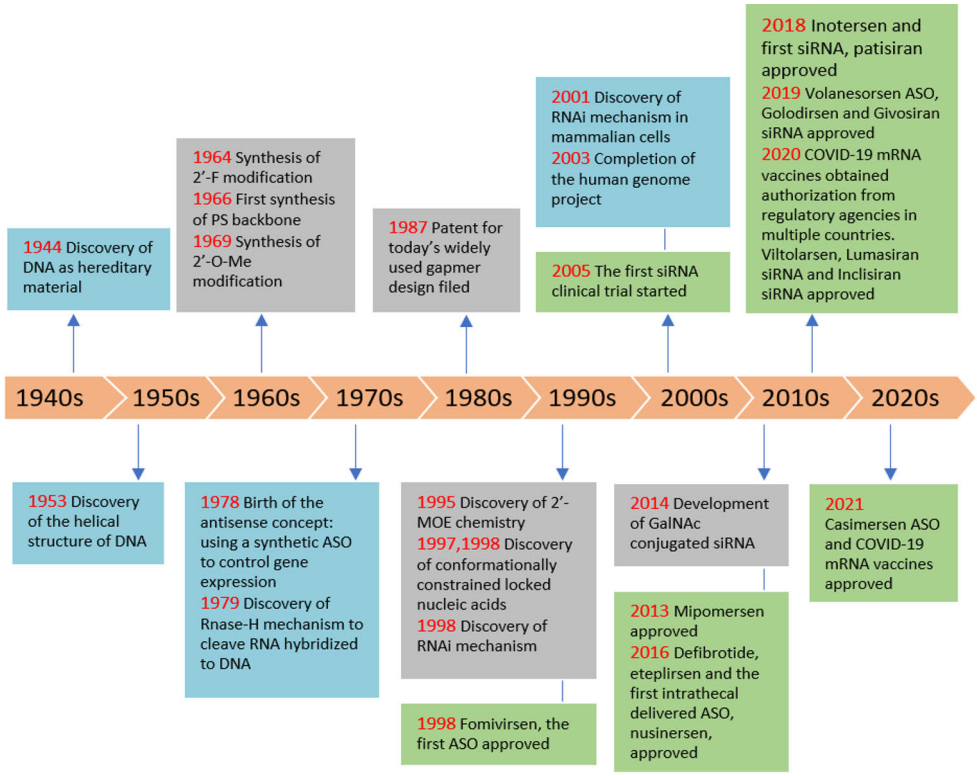

Figure 2. Timeline of selected key milestones in the development of oligonucleotide therapeutics. Blue box: milestones in biology; Grey box: milestones in chemistry; Green box: clinical milestones.

1.1.1 The essential mechanisms of action by therapeutic oligonucleotides

ASOs that activate RNase H are typically ca. 20 nucleotides long single-stranded synthetic ONs designed to bind specifically the target sequences of mRNA via Watson-Crick base-pairing to form DNA-RNA-heteroduplexes (**Figure 3**). The DNA-RNA-heteroduplex is a substrate for RNase H enzyme. RNase H cleaves the phosphodiester bonds of the target mRNA, whereas the ASO with an artificial phosphorothioate backbone remains intact and is released for hybridization with another target mRNA. Thus, a catalytic turnover may take place. The translation can be inhibited by the steric blocking of mRNA,[26] but without similar catalytic turnover. ASOs that activate RNAse H are often gapmers, means that they are hybrid sequences of both 2'-deoxyribonucleotides and ribonucleotides (2'-*O*-modified). A 2'-deoxyribonucleotide stretch (called a ``*window*'', 8-10 nucleotides long) is introduced in the middle of sequence to gain required RNAse H-activation and 2'-*O*-modified ribonucleotides, for example constrained ethyl (cEt) or 2′-*O*-

methoxyethylribose modified ribonucleotides, are introduced to both 3'- and 5'-ends. These modified stretches (ca. 5 nucleotides) are called *"wings"* of the ASO. The wings increase affinity to a complementary RNA and stabilize the ASO against nuclease-mediated degradation.[27] FDA approved ASOs based on RNAse H-mediated mRNA cleavage are Fomivirsen, Mipomersen, Inotersen, and Volanesorsen. Except Fomivirsen all are gapmers.

Splice-switching oligonucleotides (SSOs) are short, synthetic, chemically modified ONs designed to bind precursor messenger RNA (pre-mRNA). In the splicing process, the introns of pre-mRNA are removed and exons are joined to generate mature mRNA (**Figure 3**). Splicing can be altered by the hybridized ONs, which may prevent incorrect splicing and restore the formation of correct mRNA. For the clinical use, FDA has approved five SSOs. These are Nusinersen, Eteplirsen, Golodirsen, Viltolarsen, and Casimersen. The mechanism does not require similar heteroduplexes in RNase H-activation, there is more freedom to chemical modifications of the SSOs. As mentioned above, all nucleotides in Nusinersen are 2'-*O*-methyl ribonucleotides, whereas Eteplirsen, Golodirsen, Viltolarsen and Casimersen are phosphorodiamidate morpholino oligomers.

RNA interference (RNAi) was discovered for the first time in the *Caenorhabditis elegans worm* in 1998.[28] It was found that the double-stranded RNAs (dsRNA) mediate downward gene expression more efficiently than a single stranded antisense or sense RNAs. siRNAs are 20-25 nucleotides long, double-stranded ribonucleic acids contain two nucleotide overhangs at both 3′-OH and 5′-phosphate terminus.[29–31] In the cytoplasm, siRNAs bind to RNA induced silencing complex (RISC) via Argonaute protein complex[32] resulting in duplex unwinding and degradation of passenger strand (sense strand). The loaded RISC complex recognizes the target mRNA that is complementary to guide strand (antisense strand). The mRNA is then cleaved by Argonaut protein complex (**Figure 3**).[33] siRNAs have shown effective tools for RNAi-mediated target-specific gene silencing.[34] So far the four siRNA drugs, Patisiran, Givosiran, Lumasiran and Inclisiran have been approved by FDA for clinical use.

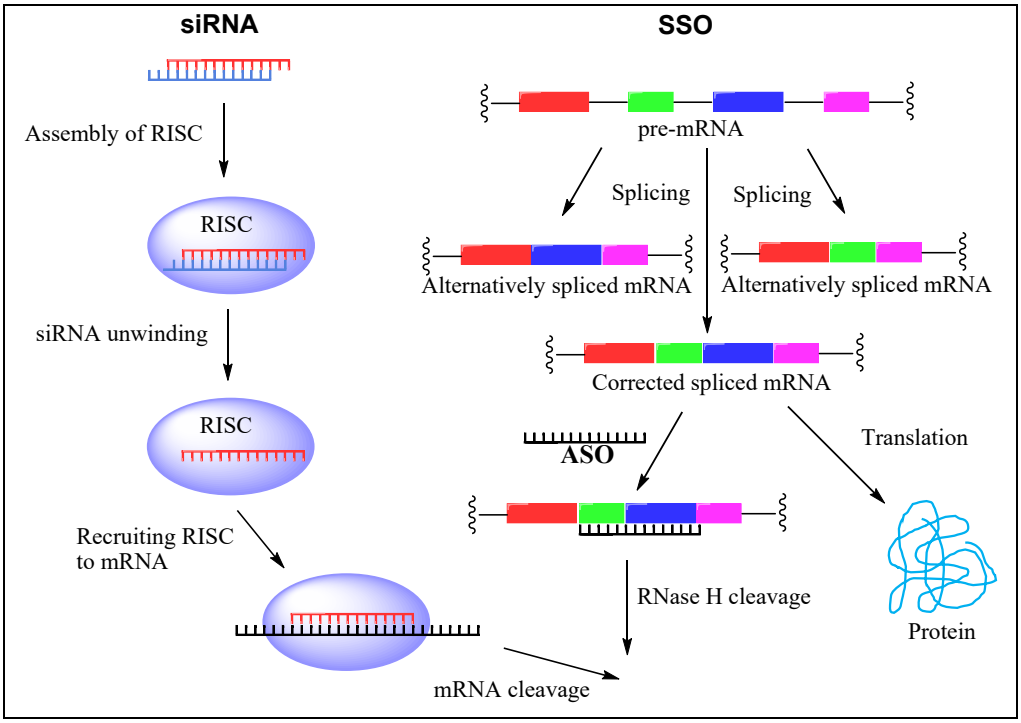

Figure 3. Therapeutic ONs mechanism of action: Splice-switching ONs, Antisense ONs, and siRNA.

1.2 Delivery of oligonucleotide therapeutics

1.2.1 Small molecule-oligonucleotide conjugates

Small molecule drugs with strong binding affinity to their receptors have been employed for ON delivery. For example, mono- and trivalent anisamide conjugates of SSOs have been prepared. Anisamide is a small molecule ligand that binds sigma receptors.[35] Sigma receptors (σ_1 and σ_2) are transmembrane proteins, present on the plasma membranes and endoplasmic reticulum. The cellular uptake of these conjugates was evaluated with human prostate carcinoma cells (PC3) which contain a luciferase reporter gene. The cellular uptake of trivalent-anisamide conjugate was significantly higher than the unconjugated SSO and mono-anisamide conjugate. Another example is folic acid (folate) that binds to folate receptor, upregulating in many human tumor cancer types. The folate polyethylene glycol siRNA (folate-PEG-siRNA) conjugate was synthesized.[36] The conjugate was shown specifically internalized into folate receptor expressing human epithelial carcinoma cells (KB cells). Following the same strategy, arachidonoyl ethanol amide (anandamide)-

siRNA conjugate targeted to cannabinoid receptor. It has been synthesized and its facilitated internalization to both neuronal and immune cells are demonstrated.[37] The conjugates have shown the similar gene silencing efficacy than corresponding unconjugated siRNAs with cationic transfection reagents.

1.2.2 Lipid-oligonucleotide conjugates

Covalent conjugation of ONs with lipid molecules have shown improvement in cellular uptake, nuclease resistance and binding to serum proteins.[38–40] For example, cholesterol-conjugated siRNA, downregulating apolipoprotein B (apoB), has shown efficient gene silencing in mice after systemic administration.[41] Recently, Nagata T. et al. reported a cholesterol-conjugated DNA/RNA heteroduplex that could cross the blood-brain barrier (BBB) and downregulate metastasis associated lung adenocarcinoma transcript 1 (Malat1) RNA in the central nervous system (CNS) after intravenous or subcutaneous administration in rats and mice.[42] Other lipophilic molecules have also been used to improve siRNAs' delivery. For example, α-tocopherol (vitamin E) conjugated with a siRNA reduced the apoB in the mouse liver.[43] Upon cellular uptake, this conjugated siRNA was cleaved in the cell by Dicer to produce the mature form of 21/21-mer siRNA after cleaving α-tocopherol. Likewise, siRNA conjugated with long-chain fatty acids were able to silence apoB.[44] Recently, docosanoic acid (DCA) conjugated siRNAs enabled for functional distribution to a variety of tissues, including heart, muscle, adrenal glands, fat and lungs, without causing toxicity.[45,46]

1.2.3 Carbohydrates-oligonucleotide conjugates

Carbohydrates play a vital role in the biological processes such as cell-cell communications, inflammation, and pathogenesis through recognition with carbohydrates-binding proteins, i.e. lectins, located on surface of the cells in most of the living organisms.[47–51] Sufficient lectin-carbohydrate recognition for plausible targeted drug delivery application needs simultaneous interaction of multiple carbohydrate units. This enhanced affinity obtained by multiple carbohydrate units is known as *glycocluster effect*.[52] For example, at least three *N*-acetylgalactosamine ligands are needed to provide sufficient delivery of ONs to asialoglycoprotein receptors (ASGPR) in hepatocytes.[53] In addition to delivery, cellular uptake is enhanced via receptor-mediated endocytosis.[54]

In early studies trivalent GalNAc cluster was covalently conjugated with methylphosphonate and phosphorothioate ONs by a neoglycopeptide linker. The cellular uptake of these conjugates by receptor-mediated endocytosis was evaluated

in the mouse models. The liver uptake could be enhanced ca. 70% compared to the non-conjugated ON.[55,56,53,57] Likewise, a trivalent GalNAc conjugate of 2′-*O*-methoxyethyl gapmer ON has shown 10-fold enhanced potential for suppressing gene expression in mouse liver.[58] In addition to the targeted delivery of single stranded ONs, the same approach can be used for delivery of siRNAs. The alignment and scaffold architecture of the GalNAc ligands don't play marked role in delivery. For example, siRNA-GalNAc-conjugates in **Figure 4A** and **4B** have equivalent hepatocyte targeting potential *in vivo* and *in vitro*.[54,59] Givosiran was the first FDA approved (in 2019) GalNAc-conjugated siRNA drug. It is a 21-mer RNA duplex with a two-nucleotide overhang at the 3′-terminus on the guide strand. The 3′-terminus of the guide strand has a trivalent GalNAc cluster conjugate group to target drug to ASGPR in liver. The nucleosides are either 2′-deoxy-2′-fluoro or 2′-*O*-methyl derivatives, which make the siRNA stable toward nuclease degradation. Givosiran regulates hepatic 5-aminolevulinic acid synthase 1 (ALSAS1) for treatment of acute hepatic porphyria (AHP), a genetic disorder that can cause harmful attacks on the nervous system. Since 2019, FDA has approved two other siRNA-GalNAc conjugate drugs (Lumasiran and Inclisiran) for clinical use.

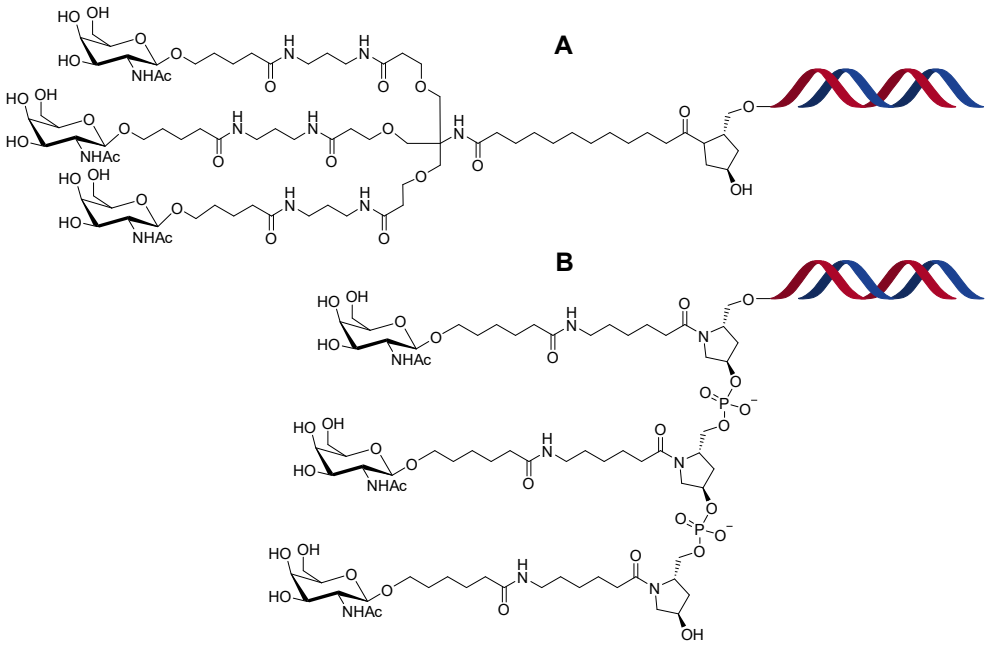

Figure 4. GalNAc-siRNA conjugates used to deliver hepatocytes via asialoglycoprotein receptors.[54,59]

In addition to GalNAc, glucose-conjugated ONs have shown the cell surface uptake and internalization through glucose transporter (GLUT) receptor mediated endocytosis.[60,61] In this study it was found that the longer spacers (15-18 atom length) facilitated internalization more than the shorter ones (4 atom length) and tetravalent glucose-conjugated ON did not improve the uptake. Other carbohydrates, including sialyl,[62] mannose-6 phosphate (M6P)[63] and hyaluronic acid[64–66] have been conjugated to ONs for targeted delivery to cells via CD22 receptor,[62] M6P/insulin-like growth factor-II receptor[63] and CD44 receptor[64], respectively.

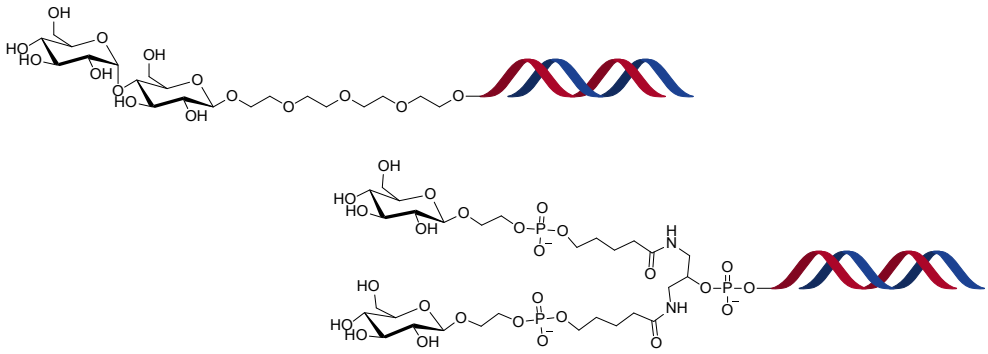

Figure 5. Glucose-siRNA conjugates.[61]

1.2.4 Antibody conjugates

Antibodies (Ab) bind with high specificity to various antigens and show attractive pharmacokinetic profile considering their applicability as the drug delivery carriers. Their applicability for the targeted delivery of small molecular drugs, especially toxins, has extensively been studied. The toxins can be specifically delivered to antigen expressing cancer cells, minimizing systemic exposure and consequently toxicity to healthy cells.[67] For example Brentuximab Vedotin is an antibody-drug conjugate, approved by FDA for treatment of relapsed Hodgkin lymphoma and systemic anaplastic large cell lymphoma.[67] It selectively targets CD30 antigen expressing tumor cells. The Ab-mediated ON-delivery is still in the early phase of its development, but some encouraging results have been reported. For example, a phosphorothioate ASO has been conjugated via a disulfide-linkage to a monoclonal Ab, selective for a CD19 receptor, and used to treat leukemia cells in vitro and in a mouse model. A specific and efficient gene silencing in leukemia cells has been obtained both in vitro and in a mouse model.[68] In another study, ASO that selectively target MAX dimerization protein 3 (MXD3) has been conjugated with an Ab (αCD22). MXD3 protein knockdown and leukemia cell apoptosis were obtained in vitro.[69] ASOs that down-regulate renal cell carcinoma (DRR/FAM107A) have been

conjugated with anti-CD44 monoclonal Ab and used to downregulate a key gene in glioblastoma stem cells in vitro.[70] Monoclonal antibody (mAb) that have binding affinity to transferrin receptor 1 (TfR1) has been conjugated with a siRNA. This Ab-siRNA-conjugate decreases levels of dystrophia myotonica protein kinase (DMPK) in skeleton muscle. An ASO conjugated to a fragment antigen-binding (Fab)-protein has been used to target the genetic basis of myotonic dystrophy type 1 (DM1) by reducing the levels of mutant DMPK .[71]

1.2.5 Aptamer conjugates

Aptamers (considered as "chemical antibodies") are relatively short ONs (DNA or RNA-sequences) that can be designed to bind efficiently to cell surface-specific biomarkers. Aptamers have been developed for the first time in 1990 by using the systematic evolution of ligands by exponential enrichment (SELEX) technique.[72] Aptamers have several benefits over antibodies. For example, they can be chemically synthesized, and the synthesis is scalable, they are chemically more stable (DNA aptamers), their site specific modification is straightforward, and they show lower immunogenicity and toxicity.[73] PSMA (prostate cancer specific membrane antigen)-specific aptamer-siRNA-conjugate was used to downregulate polo like kinase 1 (PLK1) and B-cell lymphoma 2 (BCL2) and inhibit tumor growth in prostate cancer cells.[74] The same aptamer[75] was conjugated with another siRNA that downregulate LNCaP (lymph node carcinoma of the prostate) human prostate cancer cells, and employed in mouse model via systemic administration. A pronounced regression of PSMA-expressing tumors was obtained. The antitumor activity of this aptamer-siRNA conjugate was improved later by PEG conjugation.[76] An aptamer that binds specifically to a HIV-1 envelope protein (gp 120) was conjugated with siRNA that activates sequence-specific degradation of HIV RNAs and evaluated in a humanized mouse model, in which HIV-1 replication resembled the condition in HIV-infected humans. The aptamer-siRNA conjugate showed an extensive inhibition and promise antiviral activity.[77] Recently, nanoparticles functionalized by aptamers and microRNAs have been demonstrated for treatment of the lung cancer cells.[78] Enhanced aptamer-mediated delivery to lung cancer cells and knockdown of Bcl-xL (B-cell lymphoma extra-large) protein and, consequently, induced apoptosis were observed.

1.2.6 Nanoparticles

Nanoparticles of particle size between 10-100 nm have a great potential in drug delivery. Due to small sizes, nanostructures have unique physiological and biological properties that make them a good material for biomedical applications.[79]

Nanoparticles are being utilized to address a number of issues of the delivery, including cellular uptake, tissue/cell-specific targeting, biodistribution and protection of payloads against enzymatic degradation.[80] A range of materials have been studied as nanoparticular vehicles for nucleic acids, such as liposomes,[81] micelles,[82] gold,[83] silica,[84] polymeric nanoparticles (dendrimers (polyamidoamine, PAMAM)[85] and poly(lactide-co-glycolic acid)[20] (PLGA)), DNA nanostructures,[86] and SNAs[87] (Chapter 1.3). In particular, lipid-based nanocarriers (LNPs) have been extensively studied. LNPs are biocompatible and due to lipophilicity, they are able to cross physiological barriers, including BBB.[88] LNP-nucleic acid formulation has reached the clinic, for example in case of Patisiran above.[89] LNP formulation has also been used for delivery of two mRNA vaccines, mRNA-1273 (Moderna) and BNT162b2/Comirnaty (Pfizer-BioNTech), to fight the global COVID-19.[90] The Moderna vaccine (mRNA-1273), is a lipid nanoparticle containing an ionizable cationic lipid SM-102 (heptadecan-9-yl 8-((2-hydroxyethyl) (6-oxo 6-(undecyloxy) hexyl) amino) octanoate), DSPC (1,2-distearoyl-synglycero-3 phosphocholine), cholesterol, and PEG-DMG (1-monomethoxypolyethyleneglycol-2,3-dimyristylglycerol with polyethylene glycol).[91] Pfizer-BioNTech vaccine, BNT162b2, is also a lipid nanoparticle, containing an ionizable cationic lipid ALC-0315 ((4-hydroxybutyl)azanediyl)bis(hexane-6,1-diyl)bis(2-hexyldecanoate), DSPC (1,2-distearoyl-sn-glycero-3-phosphocholine), cholesterol, and PEGDMA (2 [(polyethylene glycol)-2000]-N,N-ditetradecylacetamide).[91] Many other LNP-mRNA formulations have been developed and are under clinical trials for treatment and prevention of cancer, viral infections, and genetic diseases.[92] The corona vaccines represent in vitro-transcripted mRNAs, but the success of these nucleic acid-based drugs is expected to boost the drug development of synthetic nucleic acid therapeutics too. [93–95]

1.3 Spherical nucleic acids

The concept of spherical nucleic acids (SNAs), consisted of an appropriate core unit and a dense layer of nucleic acids, was introduced by Chad A. Mirkin and co-workers in 1996.[96] The first SNA was prepared by decorating a gold nanoparticle core with an excess of 3′-alkanethiol modified DNA strands.[96] Since then Mirkin and others reported variety of SNA structures, for example those prepared on metal cores [Gold (Au),[83] silver (Ag),[97] iron oxide ($Fe_3O)_4$,[98,99] platinum (Pt),[99] quantum dots (CdSe, CdSe/ZnS),[99,100] and core-shell ($Au@SiO_2$)[84]], and on metal free cores [silica (SiO_2),[84] [C_{60}]fullerene,[101] liposomes,[81] protein,[102] and PLGA[20]]. Both single and double-stranded ONs such as DNA,[12] micro-RNA,[103] siRNA,[14] RNA/DNA hybrids,[104] and modified nucleic acids such as locked nucleic acids (LNA),[105] and

peptide nucleic acids (PNA)[106] were attached to the core units. Examples of SNAs are shown in **Figure 6**. The unique properties of SNAs are defined primary by their dense nucleic acids layer, and the role of nanoparticle core (it's size and the obtained multivalency on it) serves an appropriate density for the nucleic acid strands. The density seems to correlate with internalization of SNAs into cells.[107] SNAs with gold nanoparticles (AuNPs) utilize most commonly gold particles of 10-15 nm size (**Figure 7**).[108,109] SNAs of sufficient ON density can be efficiently taken by almost any type of cells without transfection agents via scavenger-A receptor-mediated endocytosis.[6] In comparison to linear ONs, SNAs are more resistant to nuclease-mediated degradation (due to steric reasons),[7] and they (depending on the particle size) can avoid renal clearance in systemic administration.[110]

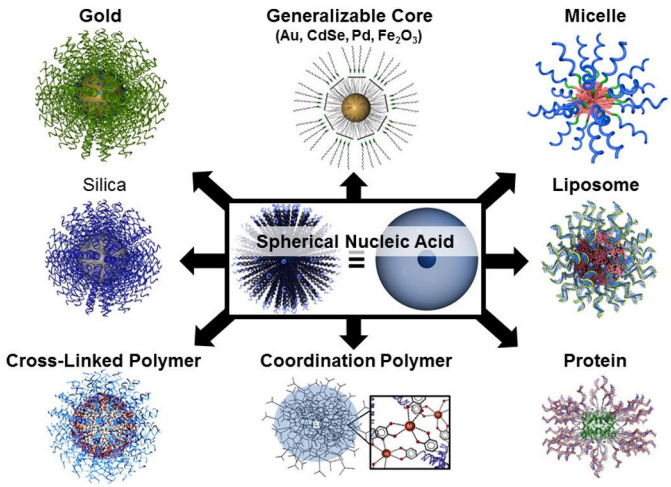

Figure 6. Different types of SNA structures based on different cores and shells. Reprinted with permission from https://mirkin-group.northwestern.edu/project/spherical-nucleic-acids/.

1.3.1 Synthesis of SNAs

AuNP-based SNAs are synthesized by mixing alkylthiol modified ONs in a solution of citrate capped AuNPs (**Figure 7**). Thiolated oligonucleotides absorb onto the surface of AuNPs and form a dense layer of ONs, due to strong binding affinity of thiol moieties to gold. [107,111] To facilitate the formation of a dense layer of ONs, the negatively charged backbones of ONs can be neutralized by adding monovalent counter ions (such as Na^+). The number of ON strands that absorb onto the AuNP surface can be controlled by changing concentration of NaCl (normally 0.15-1.0 M)

and type of spacer between ONs and the AuNP.[112] Another method reduces the electrostatic repulsion between ONs and AuNPs, by decreasing pH.[111] Also nitrogen-gold coordination can be utilized to SNA synthesis.[113] SNAs of biocompatible and biodegradable nanoparticles such as PLGAs, and proteins have been synthesized by adding dibenzocyclooctyne (DBCO)-modified oligonucleotides to azide-modified polyethylene glycol-PLGA (PLGA-PEG-N_3) in a buffer solution (0.5 M NaCl with 0.3% (v/v) Poloxamer 188 in 1X phosphate buffered saline) and azide-modified-PEG_4-protein (protein-PEG_4-N_3), respectively, via Cu-free SPAAC reaction.[20,114]

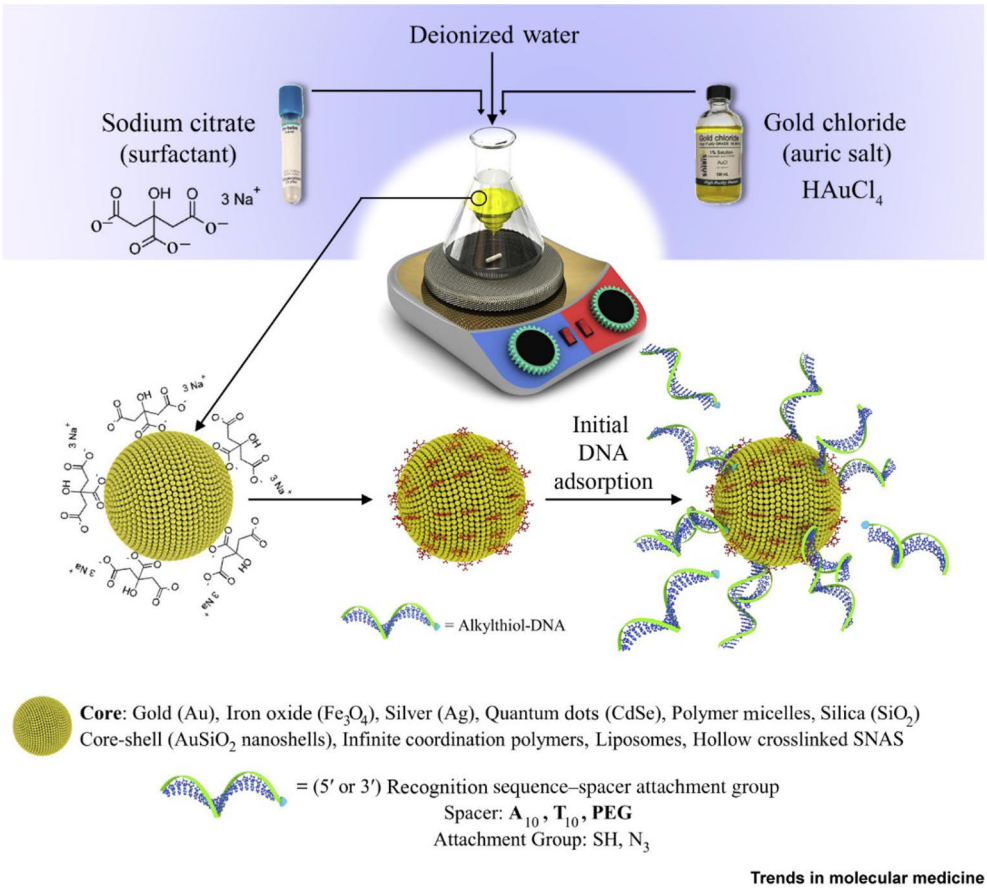

Figure 7. Synthesis of spherical nucleic acids. Reprinted with permission from Mokhtarzadeh A, Vahidnezhad H, Youssefian L, Mosafer J, Baradaran B, Uitto J. *Trends Mol Med*. **2019**; 25: 1066–1079. Copyright (2019) Elsevier.[113]

1.3.2 Applications of SNAs

1.3.2.1 Gene regulation by SNAs

Despite spherical structure and dense layer of ONs, SNAs regulates gene expression well. This was demonstrated for the first time with an SNA, consisted of 13 nm AuNP and dense layer of phosphorothioate-modified ASOs targeting enhanced green fluorescent protein (EGFP) mRNA. This SNA resulted in efficient cellular uptake, bound to the target mRNA and inhibited protein translation.[12] Since then, various types of ASO-based and RNAi-based SNAs are used to target different genes (e.g., Bcl2L12,[11] miR-182,[115] ganglioside GM3 synthase,[116] EGFR,[13,116] TNF-α,[117] Malat-1,[118] U87-MG glioma,[119] IL-17A,[120] and TLR3/9[121]). SNAs are taken up by class A scavenger receptor-mediated endocytosis.[122] After passing through intracellular endosomes, SNAs are finally released into the cytoplasm and processed by either the antisense pathway (SNAs with DNA, see section 1.1.1) or the RNAi pathway (SNAs with RNA, see section 1.1.1).[122] SNAs have already moved forward to preclinical and clinical trials, as therapeutics for skin disorders and cancers (Glioblastoma (GBM) and Triple-negative breast cancer).[122,123] For example, very recently, Kumthekar P. and et al. developed precision medicine approach for GBM treatment.[123] An SNA, in which a gold nanoparticle was covalently conjugated with a siRNA, was studied in nonhuman primate and human phase 0 clinical trials. The SNA's safety, pharmacokinetic, biodistribution and gene-knockdown were studied. The results of this clinical trial indicated that intravenous infusion of the SNA, comparable to results obtained in rats and non-human primates, were well-tolerated without long period toxicity. The SNA crossed the blood-brain barrier and blood-tumor barrier (BBB/BTB), and showed uptake into the GBM tumor cells, which associated with reduction of Bcl2L12 protein expression and induction of p53 tumor-suppressive activity.[123]

1.3.2.2 Delivery of small molecular drugs by SNAs

Chemotherapeutic drugs (e.g., cisplatin and its derivatives, paclitaxel, carboplatin, and doxorubicin) are commonly used for cancer treatments.[124] Due to the poor solubility and toxicity of these drugs, researchers have developed different targeted delivery strategies. Dhar et al. utilized AuNP-based SNAs for delivery platinum compounds.[125] The SNA was decorated by dodecyl amine-conjugated ONs, which used to carry a Pt (IV) pro drug. Different cancer cells together with healthy cells exposed to this SNA. More effective and specific apoptosis of cancer cells, in comparison to known cisplatin drugs, were noticed.[125] Similarly, Zang et al. prepared

paclitaxel-SNAs by attaching a paclitaxel carboxylic acid group to the terminal amine groups of SNA-bound ONs. An improved solubility and drug efficacy in paclitaxel resistant cell lines were observed.[126] Since these encouraging results, different SNAs strategies have been developed for delivery of other anticancer drugs, including DNA-camptothecin nanostructures,[127] DNA-paclitaxel micellar NPs,[16] doxorubicin-loaded SNAs,[17] BKM120-loaded HE_{12}-SNAs,[18] and Coumarin 6-loaded PLGA-SNAs.[20] Recently, Shuang et al. developed an SNA-based precision theranostic agent for the targeted and controlled drug delivery.[19] These results show that SNAs can be used to control the release of an encapsulated payload and provide a promising tool for chemotherapeutic drug delivery, potentially opening new paths for cancer therapy.

1.3.2.3 SNAs as molecular diagnostics

Mirkin and et al. have reported an SNA-based bio-barcode approach to detect DNA and protein targets.[128,129] Since then variety of nanoparticle based bio-barcode assays have been used to study the clinical diseases including Alzheimer's disease,[130] and prostate cancer.[131] Prigodich et al. introduced a multiplexed nanoflare for analysis of surviving levels in HeLa, MCF and Jurkat cells using AuNP-SNAs.[132] Recently, nanoflares are used as novel nanoconstructs to monitor intracellular mRNA levels as well as method for scar identification without biopsy.[132–134] Nanoflares are generated by utilizing a guide sequence with a 3′-thiol and consist of a monolayer shell of single-stranded DNA complementary to the target mRNA. The ssDNA guide sequence is pre-hybridized with a passenger flare sequence whose fluorescence is quenched when it comes into contact with AuNP. Binding of the guide sequence to the target mRNA causes displacement of the passenger flare strand, resulting in a fluorescent signal.[135,136] Recently Shuang et al. developed a reliable DNA sensor for a highly sensitive and specific detection of flap endonuclease 1 (FEN1) by using SNA and employed nanosphere as an active probe to visualize FEN1 activity in living cells and tumor-bearing mice.[19] These SNA-based nanoflares can be used for detection of different intracellular targets, such as changed mRNA levels in cancer cells and enable for in situ biomarker assay for accurate disease diagnosis.

2 Aims of the thesis

Over the last few decades, there has been a growing interest towards ONs to make an effective drug modality. Despite encouraging results, the therapeutic potential of ONs is limited by recognized problems (e.g., premature elimination via renal clearance, unfavourable biodistribution, and poor cellular uptake), which significantly limit systemic delivery of ONs to target cells. Covalent conjugation of ONs with ligands that have affinity for a specific cell type may be utilized to enhance the targeted delivery and cellular uptake of oligonucleotides via receptor-mediated endocytosis, as demonstrated by the GalNAc concept. For delivery of these ONs and ON-ligand conjugates, SNAs could be used as delivery vehicles, since they have potential to overcome the limitations of traditional nucleic acids and provide an alternative delivery method.

This thesis is focusing on improved synthetic techniques for preparation of the molecularly defined C_{60}-based SNAs, including controlled decoration strategies, synthesis of new core units and potential applicability of SNAs as hybridization-mediated carriers to enhance the glycocluster effect of sugar-conjugated therapeutic ONs.

The aims of thesis are summarized as follows:

i) To develop controlled monofunctionalization of molecular spherical nucleic acids on a [C_{60}]fullerene core.
ii) To develop glyco-decorated molecular spherical nucleic acids on a [C_{60}]fullerene core and their preliminary cellular uptake studies with PC3 prostate cancer cells.
iii) Synthesis of orthogonal multifunctional core unit and its controlled decoration with biomolecules.

3 Results and Discussion

3.1 Multipodal [C_{60}]fullerene-core units

3.1.1 Introduction

From the discovery of [C_{60}]fullerene by Kroto and et al.[137] this carbon allotrope has gained increasing attention in material science and biomedical applications due to its electrical and structural properties.[138,139] A number of synthetic methods for functionalizing fullerenes have been developed in order to increase their solubility and modify their physiochemical characteristics.[140,141] Biological studies with fullerene derivatives have shown promising results. For example, glycofullerenes (i.e., fullerene sugar balls), constructed on a hexa-substituted [C_{60}]fullerene scaffold, are potential anti-adhesive agents against the bacterial infection. Furthermore, glycofullerenes have shown promising antiviral activity in an Ebola pseudotyped infection model.[142] The synthesis of [C_{60}]fullerene hexakis adducts with a T_h-symmetry was first developed by Hirsch[143] and later modified by Sun.[144] These synthetic techniques of [C_{60}]fullerene hexakis adducts are controlled by the size of malonates and lead often to low yields. In order to solve this problem, Nierengarten and coworkers developed clickable hexakis adducts of [C_{60}]fullerene with 12 azide or alkyne terminal groups from simple malonates in high yields. The clickable hexakis adducts can be effectively functionalized by using CuAAC reaction.[145,146] Furthermore, in order to incorporate different functional components onto the [C_{60}]fullerene, they developed a two-step clickable [C_{60}]fullerene [5:1]hexakis adduct with 10 azide and 2 trimethylsilyl (TMS)-protected alkyne terminal groups by two-step synthetic procedure in high yield. This complex hexakis adduct allows the sequential attachment of 10 alkyne and 2 azide molecules through successive CuAAC reaction.[147] This synthetic technique has been used extensively in the development of new advanced materials[148,149] and bioactive molecules.[150–152] However, the use of copper (I) as a catalyst is a serious problem for compounds of biological origin. To overcome this drawback, Martin and coworkers have reported hexakis adduct of [C_{60}]fullerene with 12 cyclooctyne groups to carry out copper-free SPAAC reaction.[153] Moreover, they have described 12 maleimide hexakis adducts

of [C_{60}]fullerene for copper-free thiol-ene click reaction.[154] Then, they described two-step clickable [C_{60}]fullerene [5:1]hexakis adduct with a maleimide and 10 cyclooctyne groups to introduce two different functionalities via copper-free thiol-ene and SPAAC reactions.[154] Recently, Nierengarten and coworkers developed clickable [C_{60}]fullerene [3:3]hexakis adduct which allows sequential attachment of two different alkyne molecules via two successive CuAAC reactions.[155]

Recently, an azide-functionalized [C_{60}]fullerene is used to develop molecular spherical nucleic acids,[101,156] which is a promising method for synthesis and delivery of therapeutic ONs. This study has utilized a controlled monofunctionalization technique of molecular SNAs on the same azide-functionalized [C_{60}]fullerene. The delivery potential of this C_{60}-based SNAs was preliminary evaluated for glycocluster-oligonucleotide conjugates, resulted in efficient cellular uptake to PC3 cells. Certain biomolecular applications may need a combination of different biomolecules (i.e., hetero-antennary C_{60}-bioconjugates). For example, a drug delivery vehicle may require a system that allows orthogonal loading of tissue/cell-specific ligands and drug payloads. We have developed an azide and tetrazine-functionalized [3:3]hexakis adduct of [C_{60}]fullerene, which can be selectively one-pot functionalized by copper-free iEDDA and SPAAC reactions. By using this scaffold, assembly of hetero-antennary SNAs including glycoballs and glycopeptide structures have been demonstrated.

3.1.2 Synthesis and characterization of the C_{60}-azide core (**1**)

The synthesis of azide-derivatized C_{60}-azide core **1** has previously been reported (Scheme 1).[101] We followed the same synthetic procedure, but paid more attention to the homogeneity and authenticity of the core prior the SNA assembly. Accordingly, [C_{60}]fullerene was exposed to Bingel cyclopropanation with bis (2-(2-(2-(2-azidoethoxy) ethoxy)-ethoxy) malonate to yield C_{60}-azide core (**1**). Instead of one major product (**1**), we noticed that this reaction yielded a mixture of two major products (later identified as **1** and **2**), isolated by RP HPLC in 23 and 21% yields. These products showed equal molecular masses and very similar NMR data (**Figure 8**). Preliminary SPAAC studies were conducted to gain experimental characterization of the products. Both **1** and **2** were subjected to an excess of bicycle [6.1.0] non-4-yn-9-ylmethanol and 2-bicycle [6.1.0] non-4-yn-9-yl- (BCN) modified T_6 sequence (**ON1).** MS (ESI-TOF) analysis verified that core **1** yielded the expected fully functionalized 12-armed products, whereas reactions with **2** stacked to undeca-functionalized ones. An aliquot of **2** was then introduced to ^{1}H-^{15}N heteronuclear multiple bond correlation (HMBC) analysis, which indicated that part of the nitrogen

signals was characteristic to triazol and not entirely to alkylazide. According to this data, we concluded that [3 + 2] cyclo addition competed with desired cyclopropanation. The triazol formation is not a surprise, as this reaction has been utilized to functionalize C_{60}-core under very similar conditions.[138,142,157–159] For an additional proof, triazolino fullerenes were prepared by treating [C_{60}]fullerene with 2-(2-(2-(2-azidoethoxy) ethoxy)-ethoxy) ethanol. The NMR signals of the triazolino fullerenes (di-, tri-, and tetrafunctionalized products obtained) were equivalent to the trace signals of **2**. According to this data, we concluded that the core **1** was the expected one, with 12 azides and other major product represented the structure **2** (Scheme 1). It may be worth noting that only two major products were isolated and characterized, and we did not invest effort to identify plausible further triazol adducts in a mixture, though they are likely. Interestingly, the NMR data of **2** matched exactly with previously reported for **1** (**Figure 8**). Hence, the originally described core was wrong and we reported the correct one for the first time.

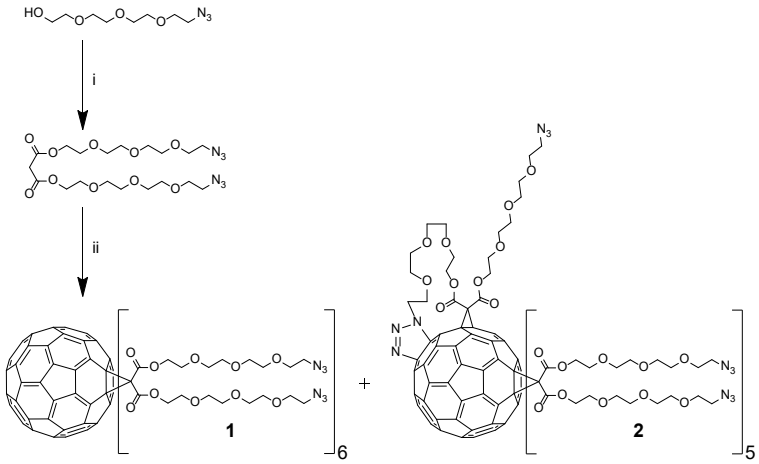

Scheme 1. Conditions: i) Malonyl chloride, $NaHCO_3$, DCM, under nitrogen, 0 °C to r.t. overnight. ii) C_{60}, CBr_4, 1,8-diazabicyclo[5,4,0]undec-7-ene (DBU), *o*-dichlorobenzene under argon, 3 days at r.t.

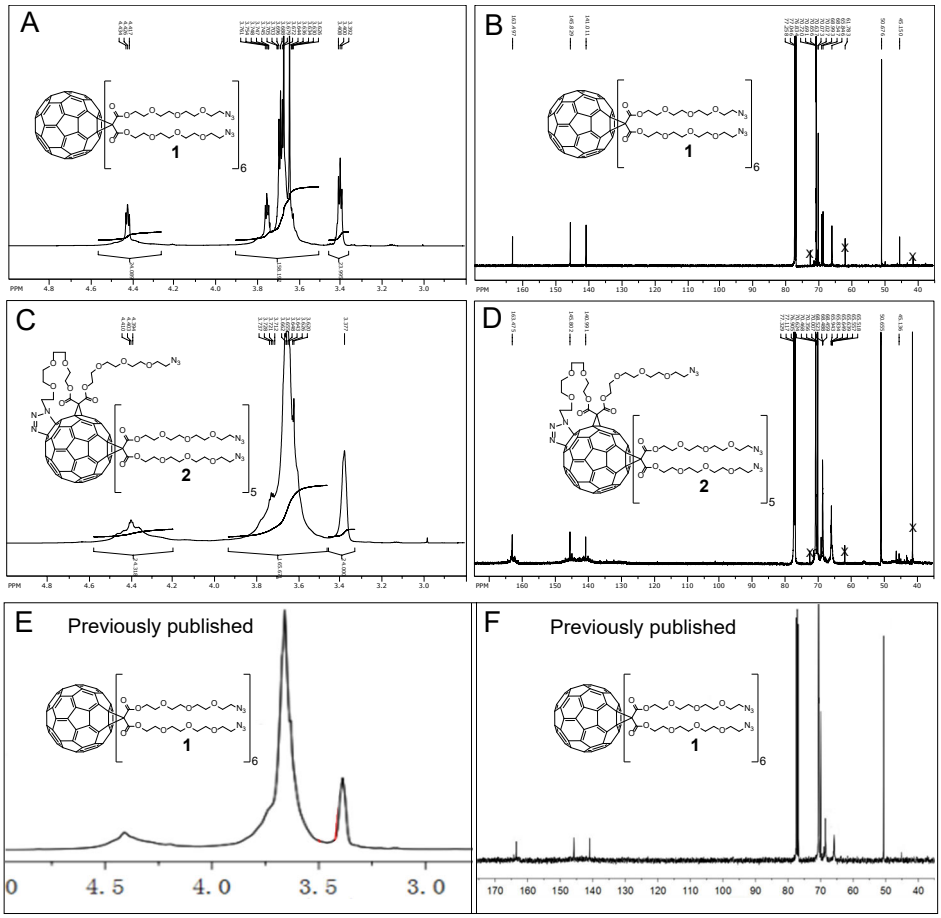

Figure 8. NMR data of 1 and 2 and comparison to previously published data. A and B) ^{1}H NMR and ^{13}C NMR spectrum of **1**, C and D) ^{1}H NMR and ^{13}C NMR spectrum of **2**, E and F) previously published ^{1}H NMR and ^{13}C NMR spectrum of **1**. As seen, the NMR data of the side product **2** matched with the data previously reported for **1**.

3.1.3 Synthesis and characterization of the bifunctional C_{60}-core (**3**)

Stepwise Bingel cyclopropanations were utilized for the synthesis of heterofunctional [C_{60}]fullerene cores. For example, controlled mono Bingel cyclopropanation of [C_{60}]fullerene, followed by full-decoration with the same reaction by using two different malonates which enabled synthesis of 5:1- , 10:1-and even 10:1:1-heterosubstituted C_{60}-scaffolds (**Figure 9**), that had used for the orthogonal ligation e.g., via alkyne-azide and thiol-ene click reactions. Recently, stereodefined C_{60} [3:3]hexa-adducts were prepared by two subsequent click reactions. For the controlled assembly, a C_{60} tris-adduct was first regioselectively

prepared using a macrocyclic malonate, which was then exposed to the Bingel cyclopropanation with another malonate (**Figure 9**).

For synthesis of C_{60}-core **3**, [C_{60}]fullerene was exposed to Bingel cyclopropanation with a heteroarm malonate **4** (Scheme 2). Instead of a Meldrum's acid-based approach, which allows a controlled stepwise reaction with two different alcohols, the one-step acylation between malonyl chloride and a mixture of alcohols **6** and **5**, 1:1, *n/n*) was used for synthesis of heteroarm malonate (**4**) in an acceptable 21% yield. Bingel cyclopropanation between [C_{60}]fullerene and **4** gave the hexakis-substituted C_{60}-core **3**. The crude material of **3** was purified first by column chromatography and then by RP HPLC to obtain the homogenized **3** in 5% isolated yield. The authenticity of **3** was verified by NMR and MS (ESI-TOF) spectroscopy. It may be worth of mentioning that while cyclopropanated C_{60}-moiety of **3** is a well-organized structure with pyritohedral symmetry, **3** is obtained as a stereoisomeric mixture (in fact $2^5 = 32$ stereoisomers) due to heteroarm malonate.

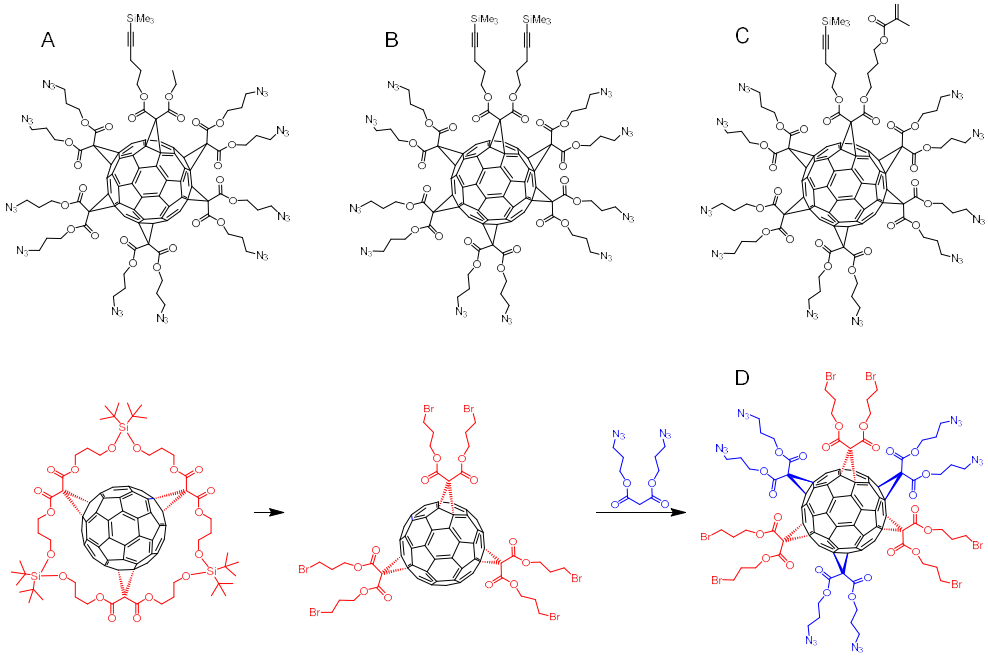

Figure 9. Examples of heterosubstituted C_{60}-scafolds. A) a 10:1-heterosubstituted C_{60}-scafold,[151] B) a 5:1-hexa-adduct C_{60}-scafold,[147] C) a 10:1:1-heterosubstituted C_{60}-scafold,[160] D) a 3:3-hexa-adduct C_{60}-scafold.[155]

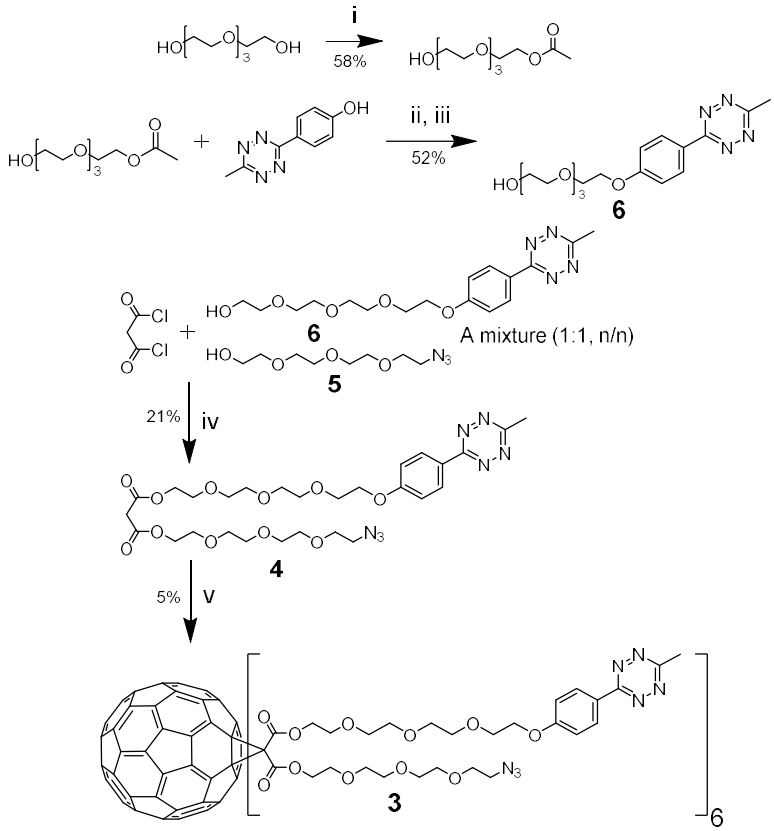

Scheme 2. Reagents and conditions, (i) Ac_2O, pyridine, 0 °C to r.t.; (ii) DIAD, PPh_3, THF, 0 °C to r.t. under N_2; (iii) 0.1 M K_2CO_3 in MeOH, r.t.; (iv) $NaHCO_3$, DCM, under nitrogen, 0 °C to r.t. overnight. v) C_{60}, CBr_4, 1,8-diazabicyclo[5,4,0]undec-7-ene (DBU), *o*-dichlorobenzene under argon, 3 days at r.t.

3.2 Controlled monofunctionalization of molecular C_{60}-based SNAs

3.2.1 Introduction

For monitoring of cellular uptake and bio-distribution of molecular SNAs, an appropriate labelling is needed. However, the label itself may contribute to the distribution and cellular delivery of the actual structure. Therefore, to keep the label effect minimal, an established method that allows controlled mono-functionalization of the SNAs might prove valuable. Furthermore, the controlled monofunctionalization can be utilized to integrate SNAs specifically with other delivery vehicles. In this thesis the azide-functionalized 12-armed [C_{60}]fullerene (**1**) could be monofunctionalized in relatively high yields (45-50%), when carefully

exposed to a substoichiometric amount of BCN-modified and labeled (DOTA and Alexa 488) ONs. The isolated intermediate products were treated with an excess of non-labelled ON constituents in an aqueous media, which gave the mono-labelled full-armed SNAs. This two-step process was crucial, not only for the controlled assembly, but also for preparation of the C_{60}-based SNAs in general. The solubility properties of lipophilic C_{60}-core and hydrophilic ONs proved to retard the full decoration in one reaction media only.

3.2.2 Oligonucleotide synthesis

For SPAAC-reactions with [C_{60}]fullerene core **1**, a set of BCN-modified ONs (**ON1-ON3** and **ON5-ON7**, Scheme 3) were synthesized. The ONs were synthesized on 1-2 μmol scale using an automated DNA/RNA synthesizer. Commercially available 2′-*O*-methylribonucleotide, 2′-deoxyribonucleotide and BCN CE-phosphoramidite building blocks and the standard phosphoramidite coupling cycle were used for assembly. For preparation of **ON3**, 3-phenyl 1,2,4-dithiazoline-5-one (POS) was used as a sulfurization reagent. Previously reported customized solid supports,[161,162] were utilized for the synthesis of appropriately 3′-modified ONs: **ON5** and **ON7** with a 1,4,7,10-tetraazacyclododecane1,4,7,10-tetraacetic acid (DOTA) and a D-galactose moiety, respectively. The **ON5** was released from solid support by two-step cleavage protocol: i) the solid support first treated with 0.1 mol L^{-1} aq. NaOH for 3 h at 55 °C, followed by neutralization with 1.0 mol L^{-1} aq. NH_4Cl. ii) overnight incubation in concentrated aq. ammonia at 55 °C. This cleavage protocol is needed to gain the desired carboxylates on the DOTA chelator. The other ONs were released from the solid support by overnight incubation in concentrated aq. ammonia at 55 °C. The **ONs** were purified by RP HPLC and characterized by MS (ESI-TOF) spectroscopy. Isolated yields were determined by UV-spectroscopy, based on molar absorptivity of ONs at 260 nm. **ON1** and **ON2**, with short model sequences, were used first to demonstrate the compatibility of the SNA assembly (**S1** and **S2**) (cf. above the chapter 3.1.2.). **ON3**-**ON7** were biologically active sequences. The phosphorothioate (PS) sequence of **ON3** (and **ON4**) is a splice switching ON that downregulates androgenic receptor variant (AR-V7) in prostate cancer cells.[163] **ON5**-**ON7** contain a 2′-O-methyl modified sequence that is complementary to microRNA 15b, involved in hepatocyte apoptosis.[164,165] Bio-distribution of this same ON sequence and its glycoconjugates have previously been studied by in vivo positron emission tomography/computed tomography (PET/CT) imaging.[66,166,167]

3.2.3 Synthesis of monofunctionalized SNAs

In primary trials, C_{60}-azide core **1** was dissolved in a small amount of DMSO and then treated with an excess of BCN-modified oligonucleotides in aqueous solution containing 1.5 M NaCl.[101] The SPAAC conjugation was retarded by drastically differing solubility properties of the lipophilic C_{60}-azide core **1** and hydrophilic ONs, resulting in complicated mixtures of products (reactions by using different DMSO-H_2O ratios, different spacers between the ONs and core, BCN- vs. DBCO-modified ONs and different temperature were attempted). This led us to try a two-step method in which **1** was initially conjugated with ONs in DMSO, and then the reaction was switched to an aqueous medium to generate full-armed SNAs after partly functionalized more hydrophilic intermediate products were achieved. Interestingly, monofunctionalization accumulated in DMSO, which could be driven further with a slight excess of **1**. This could be utilized for controlled assembly of hetero antennary SNAs (**S1-S5**, Scheme 3). In the final protocol, BCN-modified ONs (**ON1-3** and **5**) were treated with a 5 equiv. excess of **1** in DMSO (Scheme 3) to generate monofunctionalized C_{60}-ON conjugates (**C1-C3** and **C5**) in reasonably high isolated yields (45-50%). The amino-modified conjugate (**C3**) was labeled with Alexa-488-N-hydroxysuccinimide (NHS) ester. The conjugates (**C1, C2, C4** and **C5**) were dissolved in aqueous 1.5 M NaCl solution and treated with an excess (1.5 equiv./azide arm) of BCN-ONs (**ON1, ON3, ON6** and **ON7**). The reaction mixtures were purified by RP HPLC (**Figure 10**). Isolated yields (40-57%) of SNAs **S1-S5** were determined by UV-spectroscopy based on molar absorptivity of ONs at 260 nm (**S1, S2, S4** and **S5**) and at 488 nm (**S3**).

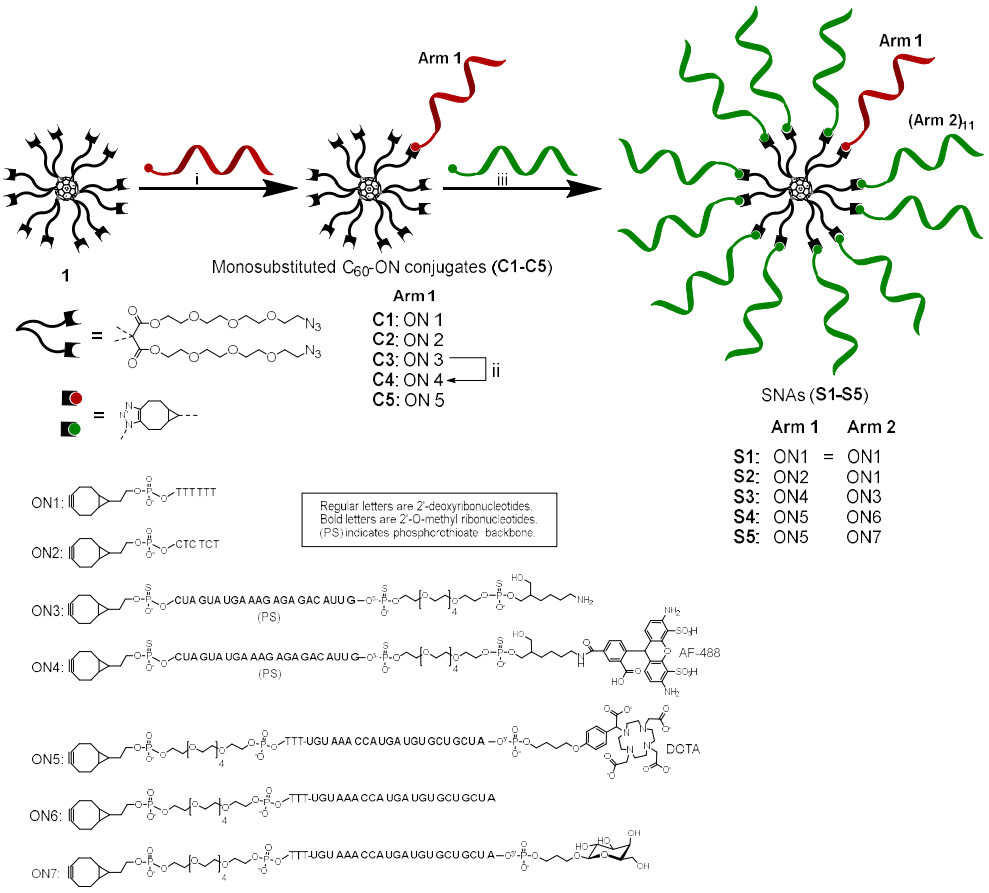

Scheme 3. Conditions: i) BCN-modified oligonucleotides (**ON1, ON2, ON3** and **ON5)**, **1** (5 eq.) in DMSO, overnight at 25°C, ii) AF-488 NHS ester (excess), 0.1 M sodium borate (pH 8.5), overnight at 25°C, iii) **C1, C2, C4** and **C5**, BCN-modified oligonucleotides **ON1, ON3, ON6** and **ON7** (1.2 eq. / arm) in aqueous 1.5 M NaCl, 3 days at 25°C.

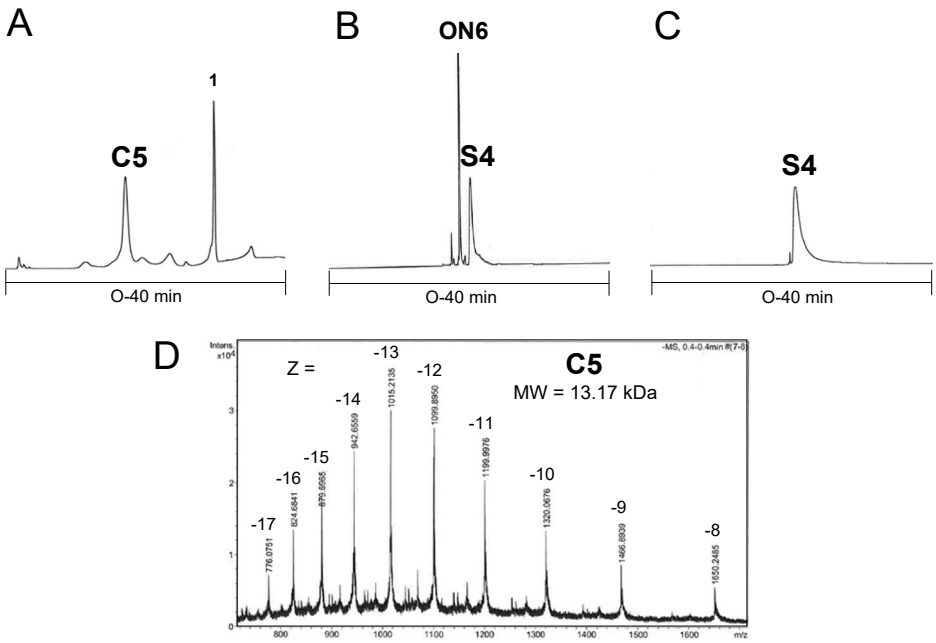

Figure 10. Example of RP HPLC profiles of crude product **C5** (A) and **S4** (B) mixtures, and purified **S4** SNA (C). (D) Example of MS (ESI-TOF) spectra of the monofunctionalized C_{60}-core (**C5**).

3.2.4 Characterization of SNAs (**S1-S5**)

3.2.4.1 Gel electrophoresis

Polyacrylamide gel electrophoresis (PAGE) was used to verify the homogeneity and identity the RP HPLC purified SNAs. Samples **S1-S5** SNAs (5 µL of 0.1 µM SNAs mixed with TBE sample buffer) and 5 µL of DNA ladder 100-1000 bp (to confirm the quality and reliability of the analysis) were loaded onto a native 6% Tris base, boric acid, ethylenediaminetetraacetic acid (EDTA), and acrylamide (TBE) gel, electrophorized, stained and imaged under G-box camera. As observed on the gel, **S1**, **S2**, **S4,** and **S5** SNAs resulted in distinct and relatively sharp bands (**Figure 11**). Additionally, faster eluting trace products were detected with larger SNAs **S4** and **S5** (< 5% of the total intensity, most likely 11-armed SNAs), indicating that the decoration was incomplete. In comparison to **S1**, **S2**, **S4,** and **S5** SNAs, **S3** resulted in a wide band probably due to stereoisomeric phosphorothioate backbone. PAGE analysis proved that the overall purity of an assembled SNAs which was rather high after single RP HPLC purification.

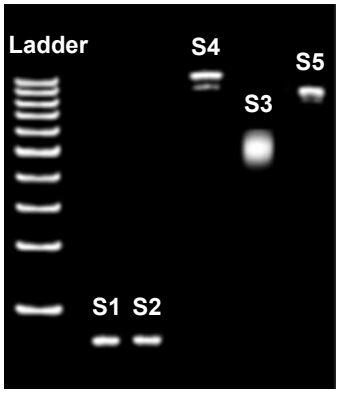

Figure 11. PAGE of **S1-S5** SNAs.

3.2.4.2 Capillary electrophoresis

Capillary electrophoresis (CE) is an efficient tool for separation of DNA fragments, based onto their size and ionic properties. We used CE to verify the purity of SNAs (**Figure 12**). CE was unable to distinguish the traces of partial (11-armed SNAs) products from full-armed SNAs, but it proved to be a useful tool to confirm the absence of free oligonucleotides (non-conjugated to C_{60}-core **1**).

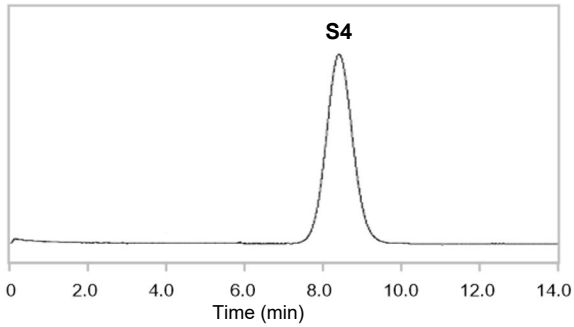

Figure 12. Example of CE of purified **S4** SNA.

3.2.4.3 Dynamic light scattering

Dynamic light scattering (DLS), is a commonly used method for characterizing dispersions of nanoparticles. We used DLS for determination of hydrodynamic diameter of SNAs. Samples 10 µg of SNAs (**S1-S5)** in 100 µL of aqueous 10 mmol L^{-1} PBS, 2.7 mmol L^{-1} M KCl, 0.137 mol L^{-1} NaCl, pH 7.4, were prepared and

measured. The hydrodynamic size of **S1-S5** ranged from 9.2 to 21.4 nm (**Table 1**), which corresponded to the lengths of component ONs.

Table 1. Hydrodynamic size of **S1-S5** SNAs.

SNAs	Hydrodynamic size/nm
S1	9.2 ± 1.2
S2	9.6 ± 2.5
S3	16.2 ± 0.1
S4	19.0 ± 2.0
S5	21.4 ± 0.8

3.2.4.4 MS and SEC-MALS analysis of SNAs

SEC-MALS (Size exclusion chromatography equipped with multiple angle light scattering detector) is a widely used method for estimating homogeneity, aggregation tendency and molecular weight of biomolecules.[168] This is especially beneficial for high molecular weight molecules (>100 kDa), and the characterization of it is hardly achievable by MS spectroscopy. This was the case also with SNAs. Small model SNAs **S1** and **S2** (**Figure 13A**, example of **S1**) produced acceptable m/z data (using a spectrometer with a hybrid quadrupole orbitrap and nano ESI ionization), but masses of overlapping multiply charged ion patterns, interfered by multiple and stable salt adducts, were observed for **S3-S5**. This MS-data was inappropriate for accurate molecular weight characterization. Even **S1** and **S2** were susceptible to forming stable multiple sodium adducts (**Figure 13A**, example of **S1**). The observed values were 0.2 kDa greater than the expected ones (**Table 2**). Therefore, to determine the molecular weights of **S3-S5** we used SEC-MALS. Each SNA resulted into a major peak (retention time between 7-9 min) that reflected 70-96% mass fraction of the sample (**S4** as an example in **Figure 13B**). The molecular weights extracted from the major peaks were estimated by MALS, which corresponded relatively well with the expected molecular weights (**Table 2**). The obtained molecular masses for small model SNAs **S1** and **S2** and the SEC-MALS data of **S3-S5** SNAs verified authenticity of the products.

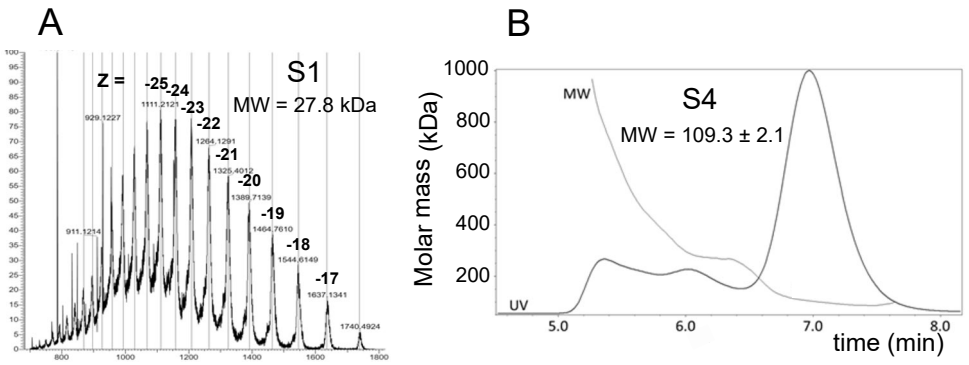

Figure 13. A) Example of the MS-ESI profile of purified **S1** SNA. B) Example of the SEC-MALS profile of purified **S4** SNA.

Table 2. Molecular masses of **S1-S5** SNAs.

SNAs	Calculated Molecular Mass/kDa	Observed Molecular Mass/kDa
S1	27.6	27.8[a]
S2	27.6	27.7[a]
S3	107.3	106.8 ± 3.6[b]
S4	109.9	109.3 ± 2.1[b]
S5	113.2	107.4 ± 2.3[b]

[a] Hybrid quadrupole-orbitrap spectrometer with nano ESI-ionization. [b] SEC-MALS.

3.2.5 UV melting studies and titration of **S3** SNA with a complementary RNA strand

Thermal stability of SNAs is an important parameter for the delivery applications. In several studies Mirkin and et al. found that the presence of gold nanoparticle probes resulted in cooperative melting properties of the target sequence, which increased the melting transition of ON-attached to the SNAs.[169–171] In contrast, later they observed that when the number of duplexed strands increased on SNAs, the melting temperature decreased, because of the steric and electrostatic repulsion between the oligonucleotide strands.[4,172–174]

To examine the hybridization characteristics of the C_{60}-based SNAs, the UV thermal melting (T_m) studies and titration of **S3** with a complementary RNA sequence were performed. As seen in the melting profiles, the T_m value of the **S3**-RNA duplex decreased, when compared to corresponding free duplex (**Figure 14A**). Furthermore, the completely hybridized **S3** (12 eq. of the complementary RNA) gave

gentler melting profiles compared to a partly hybridized one (6 eq. of the complementary RNA). This indicated an increased electrostatic repulsion/steric hindrance between the duplexes on fully loaded SNA (**S3** + 12 eq. of RNA). This observation was consistent with the earlier studies, in which RNA loading onto SNAs was retarded.[4,172–174] However, it should be highlighted that the fully loaded SNA (**S3** + 12 eq. of RNA) was nearly stable below the physiological temperature and observed premature partial denaturation occurred at a higher temperature. As the concentration of **S3** was determined using absorbance of the Alexa label (at 488 nm), stoichiometry of binding could be evaluated by a simple titration experiment, monitored by UV absorbance at 260 nm. When **S3** was titrated with a complementary RNA, overall absorbance increased with a steady slope (hypochromic effect caused by hybridization compensates the increased absorbance of the added RNA). A turning point of the slope was detected after the RNA quantity exceeded the completely occupied SNA. The measured turning point at 11.9 eq. fitted well with an expected 12:1-stoichiometry, as an additional proof of the correct SNA structure.

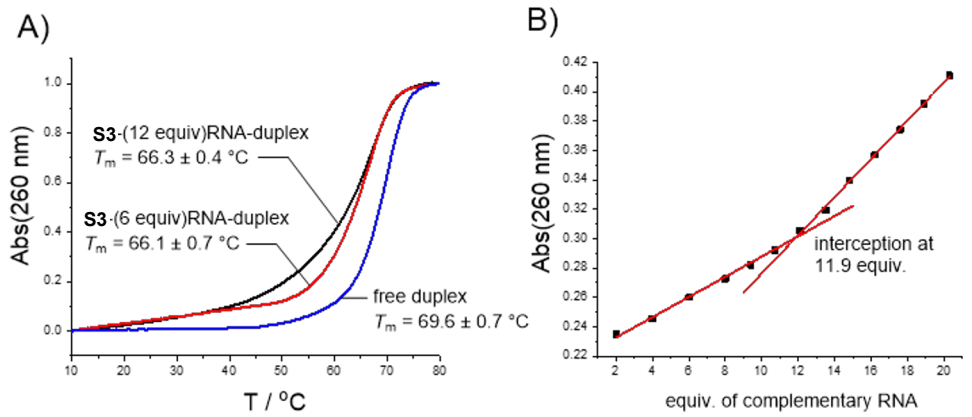

Figure 14. Melting profile analysis and titration of **S3** SNA with a complementary RNA: 5'-C AAU GUC UCU CUU UCA UAC UAG-3'. 5'-CUA GUA UGA AAG AGA GAC AUU G-3' (2´-O-methyl RNA phosphorothioate) was used to form the free duplex.

3.2.6 ^{68}Ga-radiolabeling of **S4** DOTA-SNA

Positron emission tomography imaging is a powerful tool to monitor biodistribution of drug condidates, including nanoparticular delivery vehicles. However, efficient and specific labeling of complex biomolecules with PET radionuclides may be challenging. This thesis evaluates an applicability of DOTA as a ^{68}Ga-chelating agent for SNAs. **S4** was used as a model for small-scale preliminary radiolabeling

studies. We also optimized conditions that reduced precursor loading at the expense of yield. ^{68}Ga is obtained in the form of (^{68}Ga)Cl_3 from an IGG-100 ^{68}Ge/^{68}Ga generator. The SNA **S4**, containing DOTA chelate was exposed to form ^{68}Ga complex. Up to 68 MBq of radiochemical yields were obtained (24% decay corrected yield). PAGE experiments revealed up to 69% radiochemical purity, whereas ultrafiltration recorded up to 73% purity (**Figure 15**). We found that size exclusion purification of the reaction mixture was insufficient to remove all unbound ^{68}Ga, even when two consecutive column purifications were performed. Also, commonly used solid-phase extraction columns with C8, C18 and hydrophobic lipophilic balance (HLB) solid phases were tried. We suspected unspecific binding of $^{68}Ga^{3+}$ to the SNA structure, since it was difficult to separate unbound ^{68}Ga by size exclusion chromatography. To further confirm this, the final product (**S4**[^{68}Ga]) was treated with ethylenediaminetetraacetic acid/phosphate-buffered saline (EDTA/PBS). The unbound activity percentage increased by 10% and assessed by ultrafiltration. This unspecific $^{68}Ga^{3+}$ binding to the densely packed ON construct was consistent with behavior of SNAs in MS, where relatively stable numerous sodium adducts were observed. These small-scale (1-2 nmol of precursor **S4** loading) experiments did not provide acceptable purities for in vivo imaging, but we gained useful information for future in vivo PET/CT imaging studies of SNAs. Because of the unspecific binding of $^{68}Ga^{3+}$, an indirect labeling approach, such as a click reaction with a reactive agent prelabeled with either ^{68}Ga or ^{18}F, may be a better option for SNAs.[175,176] This is later confirmed in our laboratories (unpublished results).

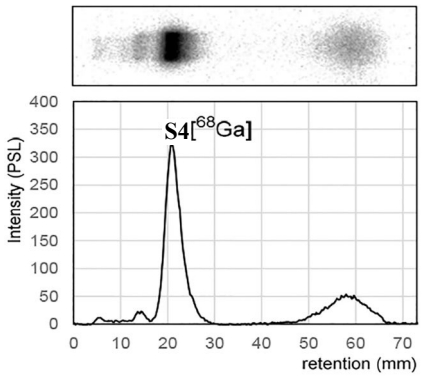

Figure 15. PAGE autoradiography image and quantification of radiolabeled **S4**[^{68}Ga] SNA.

3.3 Glycocluster-decorated spherical nucleic acids

3.3.1 Introduction

For the targeted delivery of SNAs, the radial formulation may be beneficial together with the covalent conjugate group strategy. The effect of potential cell/tissue-specific ligands may be emphasized on the outer sphere, which hide unfavorable distribution properties of the loaded oligonucleotide content inside the SNA. Furthermore, the decoration may affect the protein corona formation,[177,178] crucial for the desired bio-distribution of SNAs. Sugars deserve a special attention among the potential conjugate groups due to known interaction with proteins (such as cell-cell communication, host-pathogen interaction, immune response, and cancer metastasis) and they could potentially be applied to the targeting of ONs. The second part of the thesis describes the assembly of glyco-decorated molecular C_{60}-based SNAs, which contain trivalent clusters of bleomycin disaccharides and carbamoyl mannose as an outer decoration sphere. A splice switching ON that inhibits expression of AR-V7 in prostate cancer cells[163] was used as a payload, hybridized with a complementary carrier SNA. The bleomycin's are a class of antitumor agents, in which the sugar moiety, i.e. bleomycin saccharide (bleomycin disaccharide), is responsible for the selective tumor targeting. The internalization potential of this sugar and its monosaccharide constituent (carbamoyl mannose) has been demonstrated with different cancer cell lines (including prostate ones) in vitro.[179,180] It has also been found that the binding is based on multivalent sugar-receptor interaction.[180,181] These glycoclusters may be attractive targeting ligands to deliver ON payloads to cancer cells. [179] With an appropriate design, the required multivalency of these sugars could be obtained on the outer sphere of the SNAs. This study has utilized the hybridization-based approach to obtain the glyco-decorated nanostructures.

3.3.2 Synthesis of azide-modified bleomycin disaccharides and carbamoyl mannose

For synthesis of trivalent glycoclusters (**14**, **16α** and **16β**), azide modified bleomycin disaccharides (different anomers **9α** and **9β**) and carbamoyl mannose **11** were synthesized. The azide-modified bleomycin disaccharides **9α** and **9β** were synthesized by following the previously reported procedure (Scheme 4).[182] 2-*O*-[2,4,6-tri-*O*-acetyl-3-*O*-(*p*-nitrophenylformyl)-α-D-mannopyranosyl]-3,4-di-*O*-benzoyl-6-*O*-acetyl-L-gulopyranose (**7**) was treated with 2-(2-azidoethoxy)ethanol using triflic anhydride (Tf_2O) as a catalyst. Glycosylated compounds **8** were obtained as pure α- and β-anomers in 48 and 32% yields, respectively. Then, the active

carbonate of **8α** and **8β** was quantitatively converted to the carbamate group (**9α** and **9β**) using 0.4 N ammonia in tetrahydrofuran. The azide-modified carbamoyl mannose **11**, was synthesized from activated glycosyl donor **10,**[183] by treating it with 2-(2-azidoethoxy) ethanol in the presence of trimethylsilyl triflate (TMSOTf).

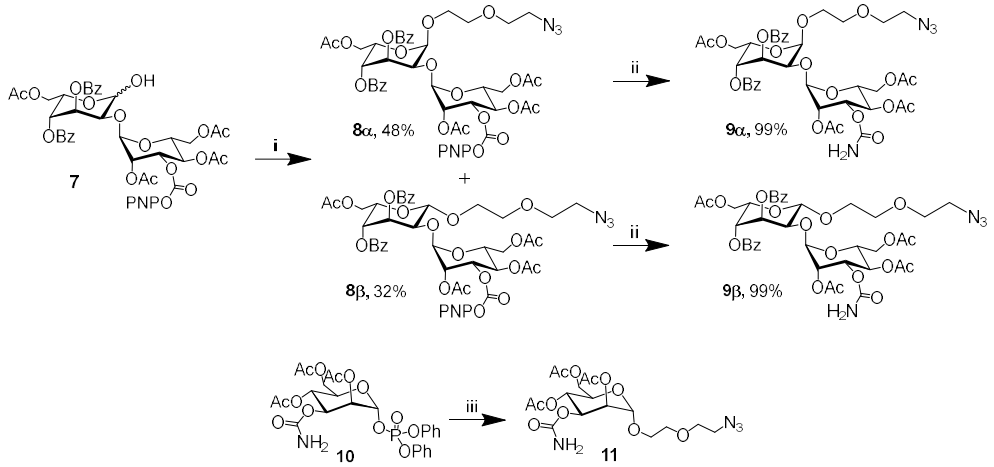

Scheme 4. Reagents and conditions: i) Ph_2SO, Tf_2O, 2,4,6-tri-*tert*-butyl pyrimidine, 2-(2-azidoethoxy)ethanol, CH_2Cl_2, -60 °C to r.t.; ii) 0.4 N NH_3 in THF, CH_2Cl_2; iii) 2-(2-azidoethoxy)ethanol, TMSOTf, O °C.

3.3.3 Synthesis of nitrone-modified trivalent clusters of bleomycin disaccharides and carbamoyl mannose

Strain-promoted alkyne-nitrone cycloaddition (SPANC),[184] was utilized for synthesis of ON-glycoconjugates (**ON12-14** below). For that purpose, nitrone-modified trivalent glycoclusters **14**, **16α** and **16β** (Scheme 5) were synthesized. The azide-modified bleomycin disaccharides (**9α** and 9**β**) and carbamoyl mannose (**11**) were joined to branching unit **12** by CuAAC reaction (Scheme 5). Then aldehyde moiety of the resulted clusters **13**, **15α** and **15β** was converted to the reactive nitrone group *in situ* by treatment with *N*-methylhydroxylamine hydrochloride. Nitrone-modified trivalent glycoclusters **14**, **16α** and **16β** were purified by RP HPLC (Scheme 5, A and B) to yield homogenized products in 47, 32 and 24%, respectively. The products were characterized by MS (ESI-TOF) and NMR spectroscopy.

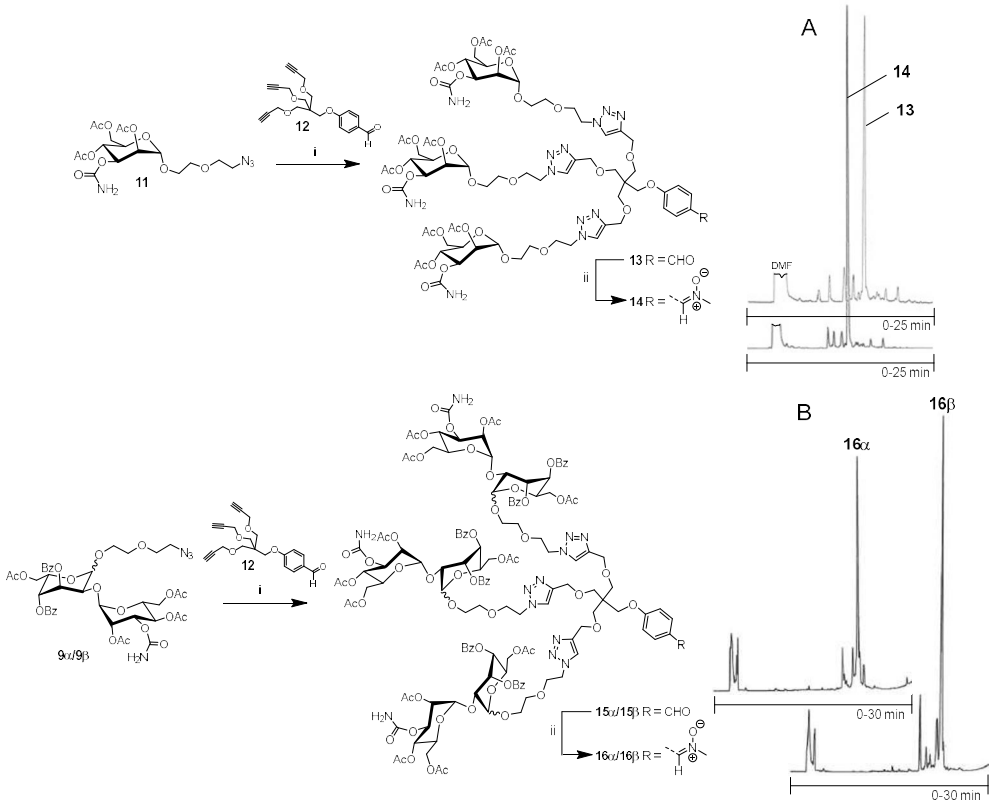

Scheme 5. Reagents and conditions: i) 0.1 mol L^{-1} sodium ascorbate, 0.1 mol L^{-1} $CuSO_4$, 1,4-dioxane, 55 °C; ii) *N*-methylhydroxylamine hydrochloride, $NaHCO_3$, DMF, r.t. (A) Crude RP HPLC profiles of **13** and **14**. (B) Crude RP HPLC profiles of **16α** and **16β**.

3.3.4 Synthesis of glycocluster-oligonucleotide conjugates

Prior to synthesis of ON-conjugates, the nitrone-modified glycoclusters **14**, **16α** and **16β** were globally deprotect by 7 N ammonia in methanol (Scheme 6). The applicability of deprotected glycoclusters **17**, **18α** and **18β** for SPANC-conjugation was then tested with commercially available DBCO-PEG4-5/6-carboxyrhodamine dye. The reactions were monitored by RP HPLC (Scheme 6, A-C) and the authenticity of expected products was verified by MS (ESI-TOF) spectroscopy. As seen in RP HPLC profiles, the reaction proceeded well, leading to virtually quantitative conversion in each case (2 equiv. dye used). After successful synthesis of these glycocluster-dye conjugates **19**, **20α** and **20β** (Scheme 6), glycocluster-ON conjugates were synthesized. A 5′-DBCO- and 3′-amino-modified 22 nucleotide long 2′-OMe phosphorothioate oligonucleotide (**ON8**) was synthesized on 2 µmol scale by using an automated DNA/RNA synthesizer. **ON8** is a splice switching ON

that inhibits expression of AR-V7 in prostate cancer cells.[163] **ON8** was treated with glycoclusters **17**, **18α** and **18β** to obtain glycocluster conjugates **ON9-11** in 11 to 17% isolated yields. Then amino moiety on the conjugates **ON9-11** was labeled with Alexa-488-N-hydroxysuccinimide ester. The reaction mixtures were purified by RP HPLC (**Figure 16**). Isolated yields of around 20 %, determined by UV-absorbance at 260 nm (**ON8-11**) and at 488 nm (**ON12-14**), were obtained. The authenticity of products was verified by MS (orbitrap) spectroscopy.

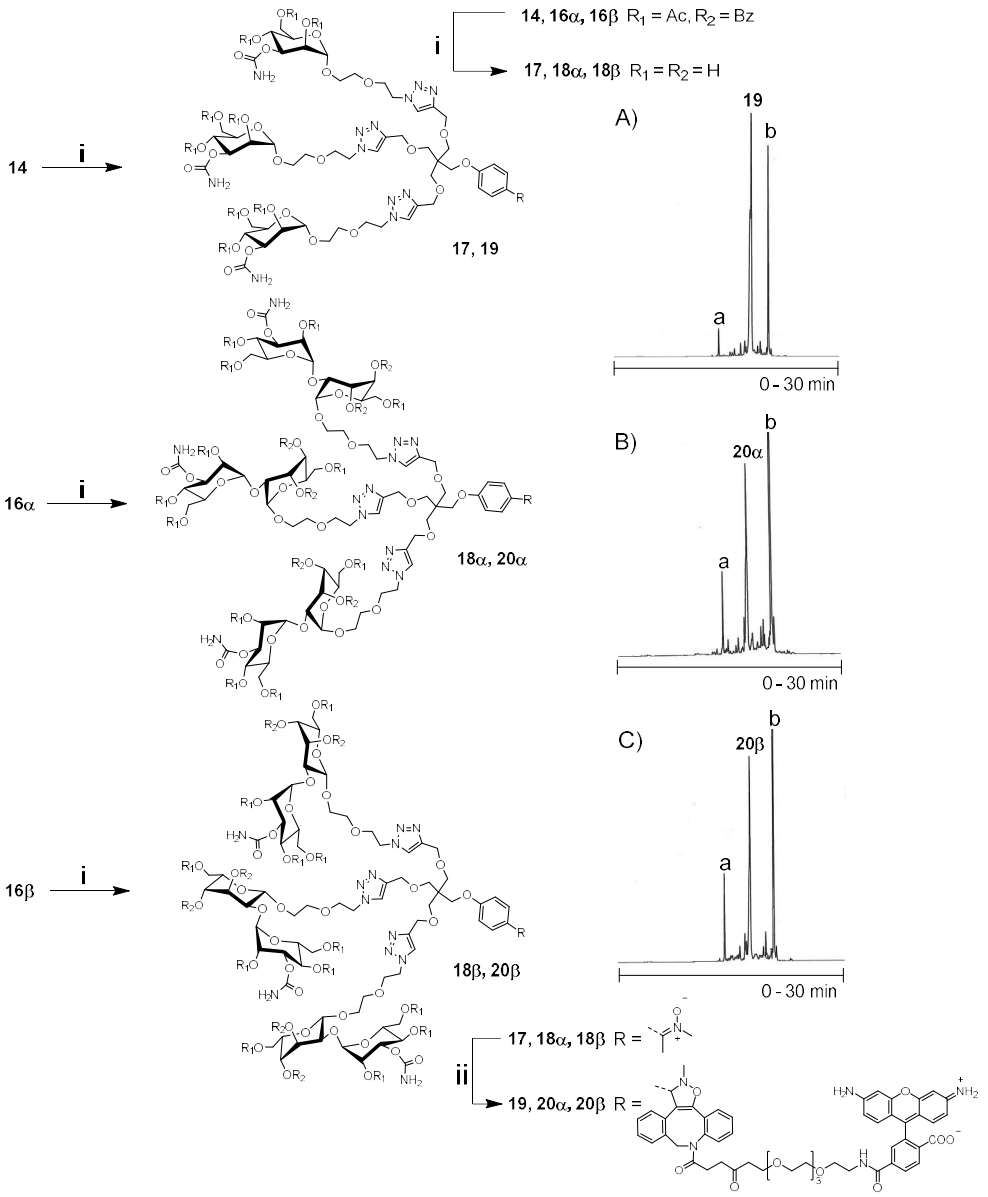

Scheme 6. Reagents and conditions: i) 7 N NH_3 in MeOH, 2 days at r.t.; ii) dibenzylcyclooctyne-PEG4-5/6-carboxyrhodamine dye, overnight at r.t.; A-C: RP HPLC profiles of the crude product **19**, **20α** and **20β**, a = byproduct of the dye, b = the dye.

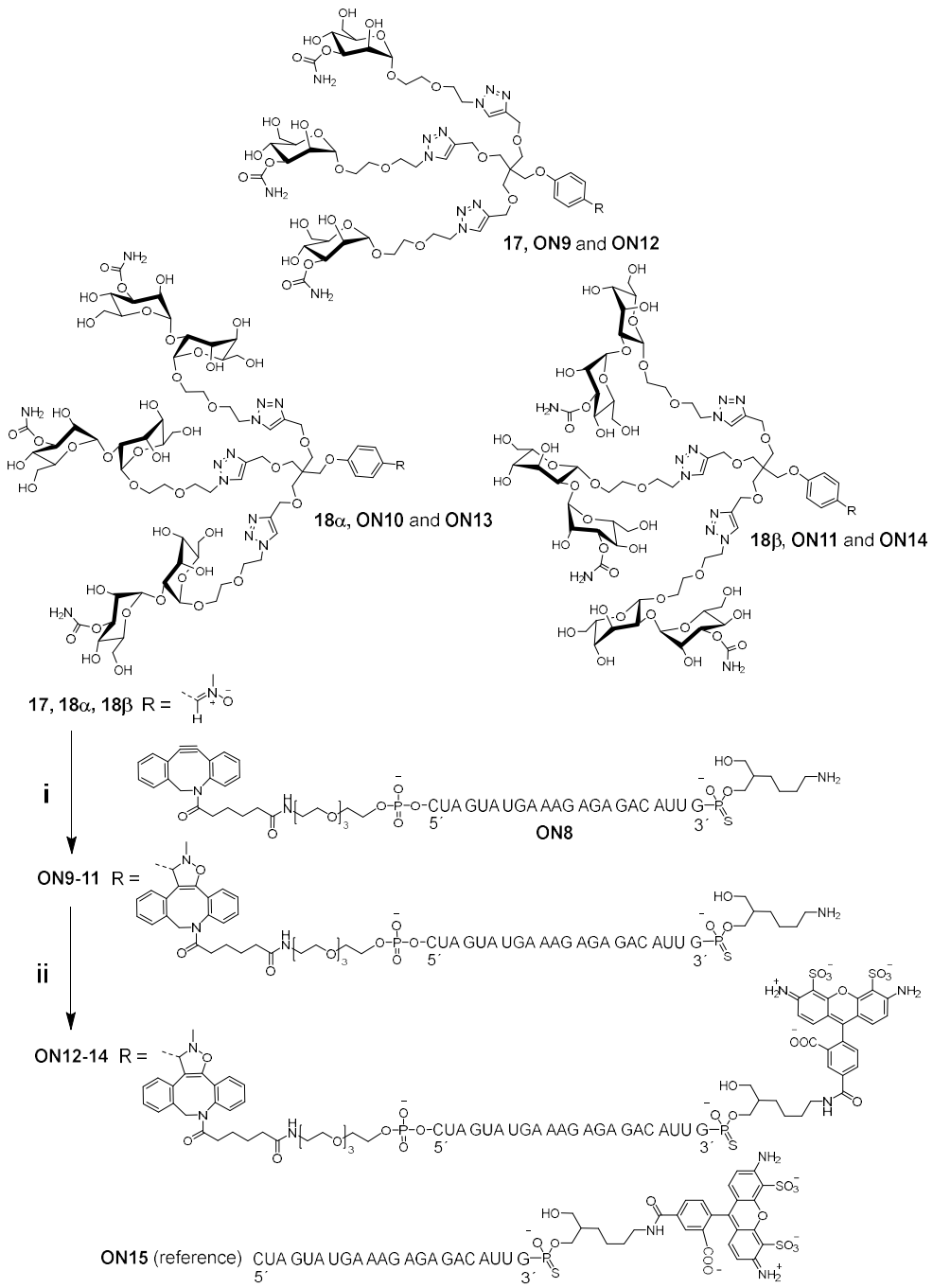

Scheme 7. Reagents and conditions: i) **ON8 + 17, 18α** or **18β**, H_2O, overnight at r.t; ii) AF-488 NHS ester, DMSO, 0.1 M sodium borate (aq, pH 8.5), overnight at r.t.

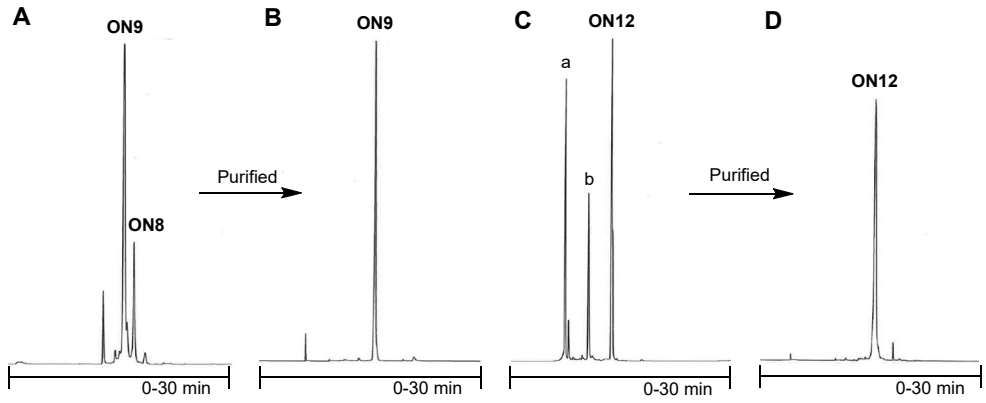

Figure 16. Example of RP HPLC profiles of crude **ON9** (A) and **ON12** (C), and purified **ON9** (B) and **ON12** (D), a and b are byproducts of the Alexa-488.

3.3.5 Assembly of glycocluster decorated SNAs

For preparation of hybridization-mediated SNAs (**S7-S10**), an SNA (**S6**) with complementary DNA strand to **ON12-15** was synthesized. **S6** was prepared in 25% overall yield by following the two-step procedure described in section 3.2.3. C_{60}-core **1** (5 eq.) was first monosubstituted by using BCN-modified **ON16** (1 eq.) in DMSO. The monosubstituted product was then treated with an excess (1.5 eq./azide arm) of same oligonucleotides (**ON16**) in high salt concentrated (1.5 M NaCl solution) aqueous media to obtain SNA **S6**. The reaction mixtures were purified by RP HPLC. The homogeneity and authenticity of **S6** was verified by PAGE (**Figure 18**) and MS (ESI)-spectroscopy, respectively (**Figure 17**). To obtain the hybridization-mediated SNAs (**S7-S10**), **S6** was exposed with **ON12-15** (12 eq.) in phosphate-buffered saline (PBS (137 mM NaCl, 2.7 mM KCl, 10 mM Na_2HPO_4, 1.8 mM KH_2PO_4) at pH 7.4). The formation and stability of the hybridization-mediated SNAs (**S7-S10**) were evaluated by PAGE, UV melting profile analysis, and time-resolved fluorescence spectroscopy.

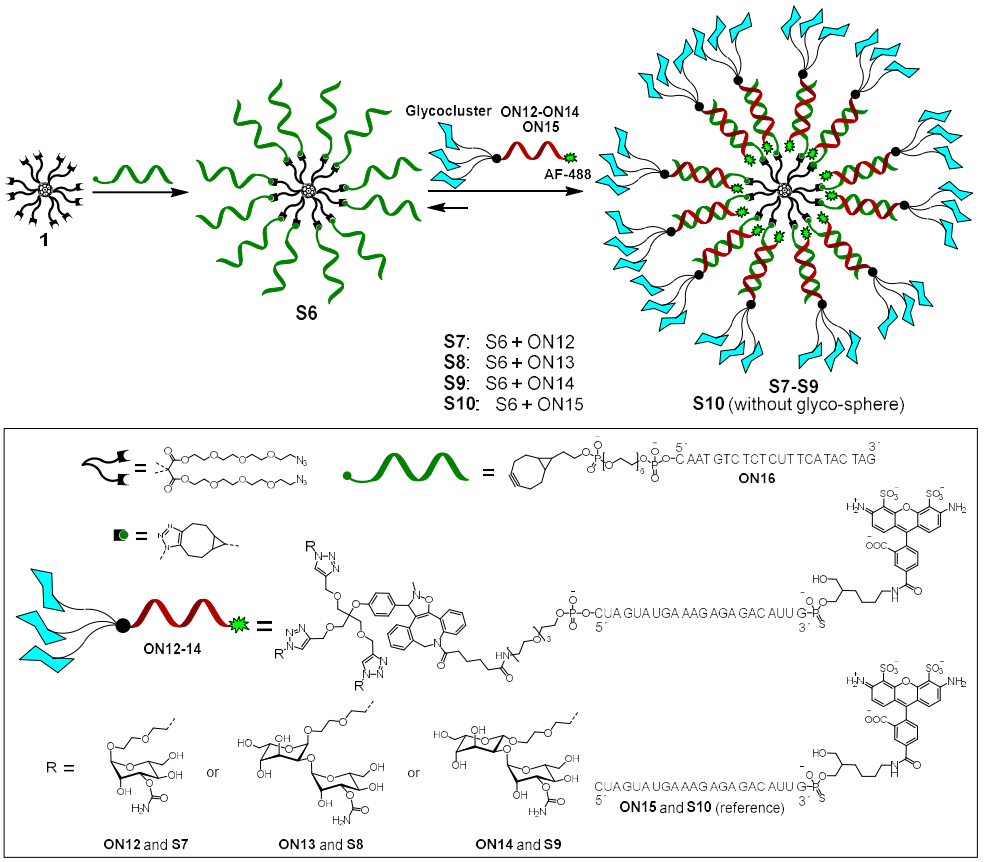

Scheme 8. Hybridization of AF-488 labeled glycocluster oligonucleotide conjugates **ON12, ON13** or **ON14** with complementary SNA (**S6**).

3.3.6 Characterization of SNAs (**S6-S10**)

3.3.6.1 MS spectroscopy of **S6** SNA

The authenticity of SNA **S6** was confirmed by MS (a spectrometer equipped with a hybrid quadrupole orbitrap and nano-ESI ionization. SNA **S6** produced acceptable m/z data (**Figure 17**), although the salt adducts interfered the accurate determination of the molecular weight (**Figure 13A**).

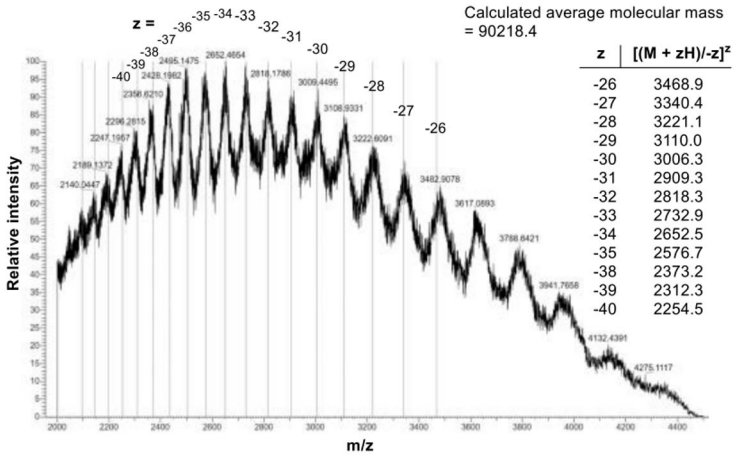

Figure 17. MS (ESI) spectroscopy of **S6** SNA.

3.3.6.2 Gel electrophoresis

PAGE was used to verify the homogeneity and identification of the RP HPLC purified SNA (**S6)** and hybridization mediated SNAs (**S7-S10**). SNA samples **S6** (5 µL of 0.1 µM SNA mixed with PBS), hybridized SNAs **S7-S10** (5 µL of 0.1 µM SNA **S6** and 12 eq. of **ON12-15** mixed with PBS**)** and 5 µL of DNA ladder 100-1000 bp were loaded onto a native 6% Tris base, boric acid, EDTA, and acrylamide (TBE) gel, electrophorized, stained and imaged under G-box camera. As noticed on the gel, **S6** SNA showed a distinct and comparatively sharp band (**Figure 18**). Mixtures of **S6** SNA with **ON12-15** showed slower eluting wide bands on the gel, indicating the formation of hybridization mediated **S7-S10** SNAs (**Figure 18**).

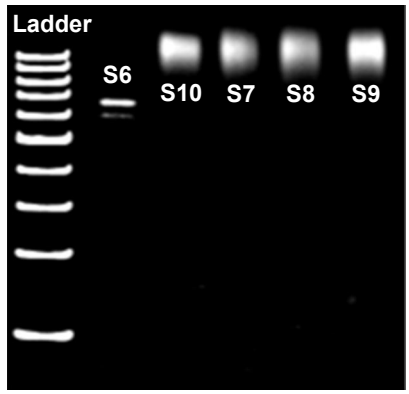

Figure 18. PAGE of **S6-S10** SNAs.

3.3.6.3 Dynamic light scattering

DLS was used to determine the hydrodynamic diameter of SNAs (**S6-S10**). Samples 10 µg of SNAs (**S6-S10)** in 100 µL of aqueous 10 mmol L^{-1} PBS, 2.7 mmol L^{-1} M KCl, 0.137 mol L^{-1} NaCl, pH 7.4, were prepared and measured. The resulting diameters of **S6-S10** ranging from 10.6 to 13.8 nm (**Table 3**).

Table 3. Hydrodynamic size of **S6-S10** SNAs.

SNAs	**Hydrodynamic size/nm**
S6	10.6 ± 0.2
S7-S9	13.8 ± 1.7
S10	11.5 ± 1.1

3.3.7 UV melting studies of hybridization-mediated SNAs

To evaluate the stability of hybridization-mediated SNAs **(S7-S10**), UV thermal melting studies were performed. Samples of **S6** (0.083 µmol) and **ON12-ON15 (**1.0 µmol, 12 eq., **Table 4**) in 10 mmol L^{-1} sodium cacodylate (pH 7.0) with 0.1 mol L^{-1} NaCl were prepared and absorbance at 260 nm over a temperature range of 10-80 °C was recorded. The UV melting curves showed inflection points at 56-57 °C. When compared to non-conjugated oligonucleotide **ON15,** the glycocluster moieties of **ON12-14** decreased the melting temperature by 1.1-1.6 °C. The glyco-moieties on the outer sphere contributed marginally to the duplex stability, as expected.

Table 4. UV melting temperatures of the SNA/oligonucleotides complexes

SNA+Ons	T_m **/ °C**
S6 + 12 eq. ON15	57.8 ± 0.9
S6 + 12 eq. ON12	56.2 ± 0.6 (-1.6)
S6 + 12 eq. ON13	56.3 ± 0.6 (-1.5)
S6 + 12 eq. ON14	56.7 ± 1.2 (-1.1)

3.3.8 Fluorescence spectroscopic analysis of hybridization-mediated SNAs

Fluorescence spectroscopy was used to study the affinity of **ON12-ON15** to **S6** in detail (collaboration with University of Tampere). The fluorescence characteristics of **S6** and **ON12-ON15** complexes are shown in **table 5**. The association constant for carbamoyl mannose conjugate **ON12** determined from time-resolved data was almost identical to that for **ON15**. The association constant for the α- and β-bleomycin disaccharide conjugates **ON13** and **ON14** was nearly half that of **ON12** and **ON15**. Complexation appeared complete for all oligonucleotides at 12:1 oligonucleotide:SNA ratio. The association constant determined from fluorescence spectra and the time-resolved data were clearly different. Only the ratios 4-12:1 or 8-12:1 was used to calculate an association constant from time-resolved data. This shows that the oligonucleotides bind initially to different part of SNA. The AF-488 fluorescence is quenched only after an oligonucleotide start to bind the adjacent strands of already occupied positions, that can be observed when fluorescence lifetime decreases.

Table 5. Association constants for the SNA/oligonucleotides complexes.

	$K_{assoc.}$ / M^{-1} (equivalents of ON/SNA)
ON12	4.64×10^6 (4–12)
ON13	2.05×10^6 (8–12)
ON14	2.24×10^6 (8–12)
ON15	5.18×10^6 (4–12)

3.3.9 Cellular uptake studies of glycocluster-oligonucleotide conjugates and corresponding SNAs

The cellular uptake studies of the **S7-S10** and corresponding **ON12-ON15** were tested with PC3 cells. Untreated PC3 cells were used as controls. **S7-S10** and **ON12-ON15** were incubated with the PC3 cells for 4 hours. After incubation, cells were washed, stained and fixed for confocal microscopy analyses. The obtained cell uptake data of the **ON12** and **S7** are shown in **Figure 19** as an example. Based on these results, it is clearly shown that the **ON12** and corresponding **S7** are taken up by the PC3 cells. It could be stated that the oligonucleotides with **S6** carrier are taken up by the cells more efficiently than those without **S6** carrier. A more detailed

mechanistic study of internalization and intracellular trafficking are ongoing in the university laboratories.

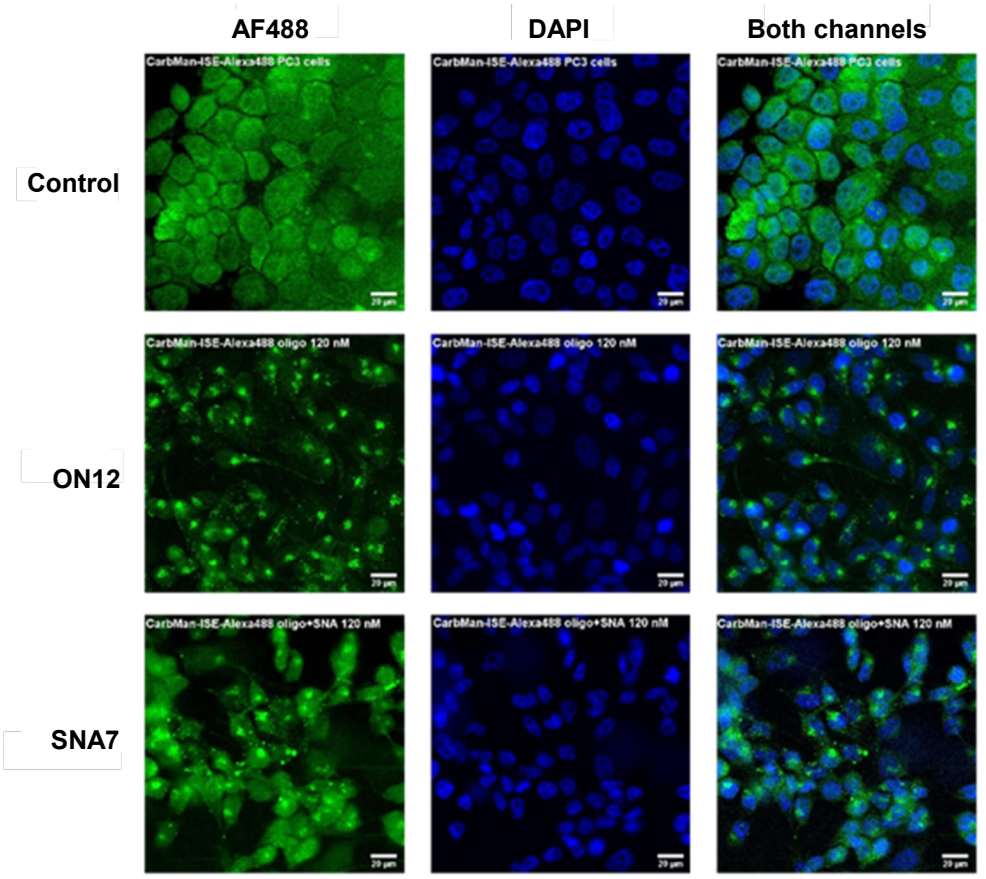

Figure 19. Cell uptake of AF-488 labeled carbamoyl mannose conjugate **ON12** and corresponding **S7** by PC3 cells. Cells were incubated with 120 nM oligonucleotide and 10 nM SNA in PBS for 4 h, at 37 °C with 5% CO_2. After incubation cells were washed by PBS, stained in 4% paraformaldehyde PBS solution and detected by Confocal and Widefield microscopy.

3.4 Controlled decoration of biomolecules on the bifunctional C_{60}-core

3.4.1 Introduction

A drug delivery vehicle may need a system that enables loading of tissue/cell-specific ligands and drug payloads in an orthogonal manner. In the third part of thesis, the azide- and tetrazine-functionalized C_{60}-core **3** can be orthogonally

functionalized by two pericyclic click reactions (i.e., iEDDA and SPAAC) in the catalyst free conditions with high isolated yields (56-69%). Furthermore, these two orthogonal reactions are compatible in one pot-assembly. The synthetic applicability of the core (**3**) for these one-pot assemblies has been demonstrated by the synthesis of heteroantennary glycoballs and one glyco-peptide C_{60} conjugate. Furthermore, a novel type of SNA, with extraordinary stable covalently bound double helices, has been synthesized by a two-step protocol in 29% overall isolated yield. This orthogonally functionalized core (**3**) may find applications in the preparation of novel C_{60}-sugar balls[142,146,150,185–187] and molecular SNAs in general.

3.4.2 Synthesis of TCO and BCN modified biomolecules

TCO and BCN-modified sugars, ONs and one BCN-modified peptide were synthesized for iEDDA and SPAAC-reactions with core **3**. p-nitrophenylcarbonate-activated methyl α-D-galacto, D-gluco and D-manno pyranoside were prepared as previously described,[188] coupled to commercially available (E)-cyclooct-4-en-1-yl(2-(2-(2-aminoethoxy)ethoxy)ethyl)carbamate and bicyclo[6.1.0]non-4-yn-9-ylmethyl(2-(2-(2-aminoethoxy)ethoxy)ethyl)carbamate by standard carbamate-coupling protocol and purified to obtain TCO and BCN modified carbohydrates. The modified carbohydrates were globally deprotected by concentrated ammonia and purified to obtain **TCO/BCN-Gal, -Glu** and –**Man** (Scheme 9). The 3′- and 5′-amino-modified ONs were purchased commercially and amino-modified peptide was synthesized by an automated peptide synthesizer. The amino modified oligonucleotides and the peptide were coupled to commercially available bicyclo [6.1.0]non-4-yn-9-ylmethyl or (E)-cyclooct-4-en-1-yl NHS carbonate via standard carbamate-coupling protocol to obtain **TCO-ON17, BCN-ON18** and **BCN-peptide** (Scheme 9). The reaction mixtures were purified by RP HPLC and characterized by MS (ESI-TOF) spectroscopy. The quantity of the obtained products was determined by UV-spectroscopy, based on molar absorptivity of ONs at 260 nm (**TCO-ON17** and **BCN-ON18**) and the peptide at 280 nm (**BCN-peptide**). The ONs were just short model sequences. The peptide was a known sequence that enhances endosomal escape.[189]

3.4.3 Synthesis of hetero-antennary bioconjugates

To evaluate the orthogonal assembly on core **3**, first C_{60}-glycoconjugate **C9** was synthesized. C_{60}-core **3** was dissolved in DMSO and exposed to iEDDA with **TCO-Gal** (9 eq., in DMSO) to yield intermediate glycoconjugate **C6**, and then **BCN-Glu** (9 eq., in DMSO) was added to the same reaction mixture. The completion of both

successive click reactions was verified by RP HPLC (**Figure 20**). The authenticity of the intermediate conjugate **C6** and the final product **C9** was verified by MS (ESI-TOF). The isolated **C9** was further characterized by NMR spectroscopy (^{1}H, COSY, HSQC, HMBC), in which the correct 1:1 ratio of the galactose and glucose units and the triazol and 1,4-dihydropyridazine moieties could be seen. Isolated yield of **C9** (66%) was measured according to ^{1}H NMR spectra by comparing the intensity of ^{1}H signals to an internal standard (a known quantity of acetonitrile used). The other heteroarmed glycoconjugates **C10** and **C11**, as well as the peptide-glycoconjugate **C12** were prepared following the same technique. The reaction mixtures were purified by RP HPLC and characterized by MS (ESI-TOF) spectroscopy. Isolated yields of **C10-C12** (56, 69 and 61%, respectively) were determined by UV-absorbance at λ = 260 nm of the products, comparing it to that of a known concentration of **C9**, $\varepsilon = 120 \times 10^3$ L mol^{-1} cm^{-1}.

After the successful synthesis of C_{60}-glycoconjugates (**C9-C12**), we verified the applicability of C_{60}-core **3** for assembly of a molecularly defined novel-type SNA, in which both strands of a double helix were covalently linked to the C_{60}-core. C_{60}-core **3** was exposed to iEDDA with **TCO-ON17** (9 eq., in DMSO) to generate hexa-armed SNA (**C13**). The reaction mixture was purified by RP HPLC (**Figure 20**) and characterized by MS (ESI-TOF) spectroscopy. Then the purified hexa-armed SNA (**C13**) was exposed to SPAAC with **BCN-ON18** (9 eq., in H_2O) to generate full-armed SNA (**C14**). The reaction mixture was purified by RP HPLC (**Figure 20**). Isolated yield of **C13** (50%) and **C14** (57%) were determined by UV-spectroscopy, based on molar absorptivity of ONs at 260 nm. Here, we did not test one-pot assembly, due to complementary strands of **ON17** and **ON18**. The homogeneity of hexa-armed SNA **C13,** hybridization mediated **SNA C15** and **C14** were evaluated by PAGE. Molecular mass of **C14** was determined by SEC-MALS.

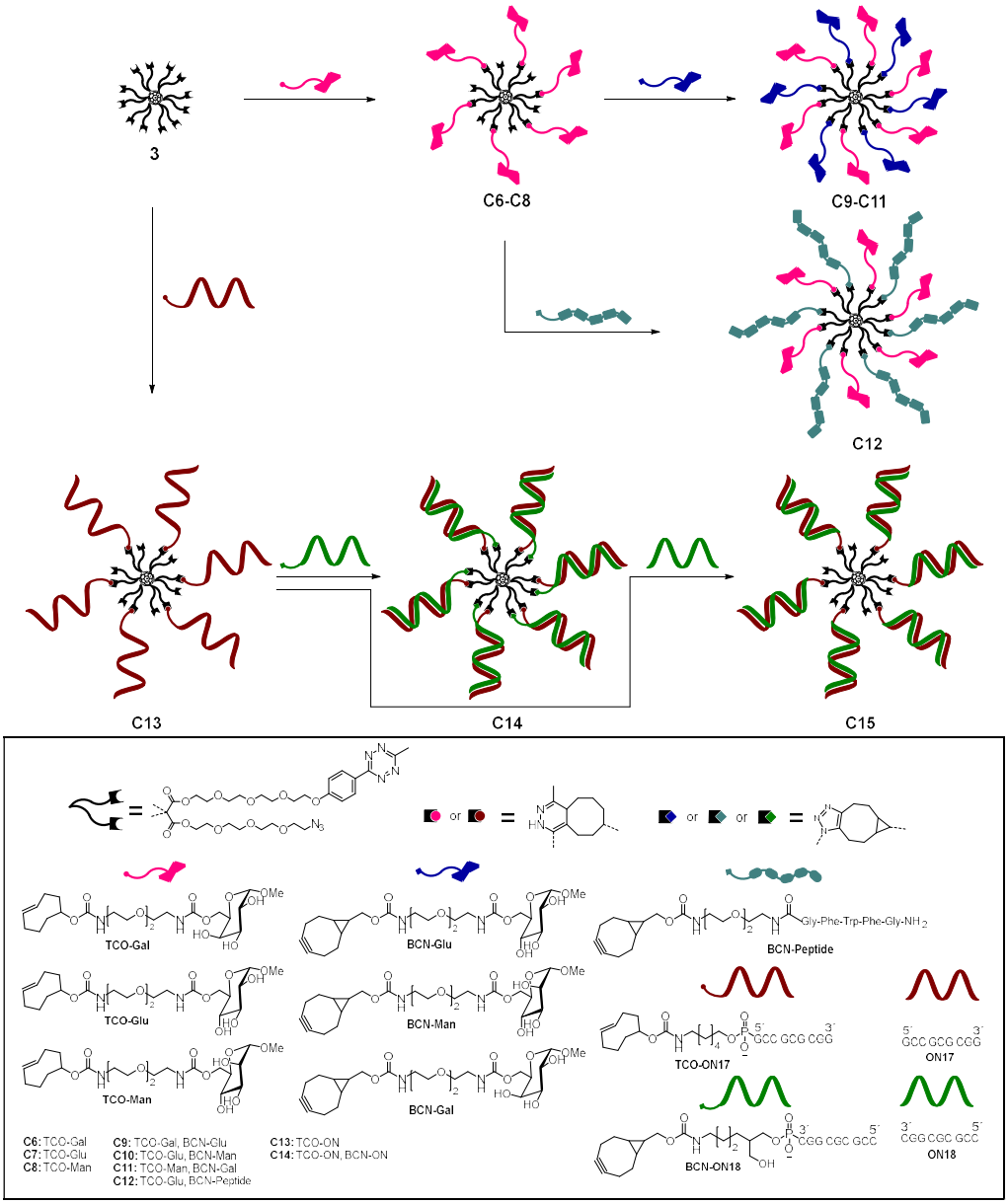

Scheme 9. Synthesis of hetero-antennary bioconjugates on bifunctional C_{60}-core **3**.

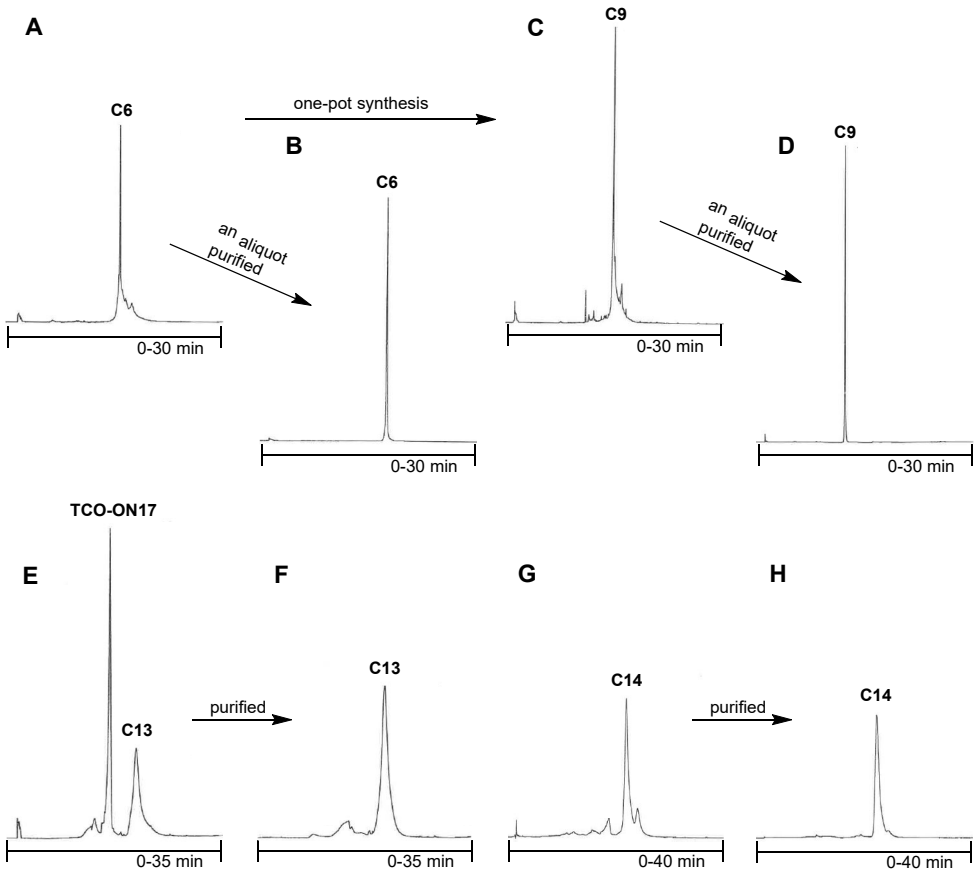

Figure 20. Example of RP HPLC profiles of crude conjugates **C6** (A), **C9** (C), **C13** (E) and **C14** (G), and purified conjugates **C6** (B), **C9** (D), **C13** (F) and **C14** (H).

3.4.4 Characterization of hetero-antennary bioconjugates (**C6-C15**)

3.4.4.1 Gel electrophoresis

PAGE was used to verify the homogeneity and identification of the RP HPLC purified SNAs **C13** and **C14**, and hybridized SNA **C15**. SNA samples **C13-C15** (5 µL of 0.3 µM SNA mixed with 6x TriTrack DNA loading dye) and 5 µL of Gene Ruler Ultra Low Range DNA ladder 10-300 bp were loaded onto a native 6% Tris base, boric acid, EDTA, and acrylamide (TBE) gel, electrophorized, stained and imaged under G-box camera. As seen on the gel (**Figure 21**), **C13-C15** SNAs resulted in distinct bands. **C14** eluted much slower than **C15**. Interestingly, the

covalent linkage of **ON18** to the C_{60}-core **3** is the only difference between **C14** and **C15**.

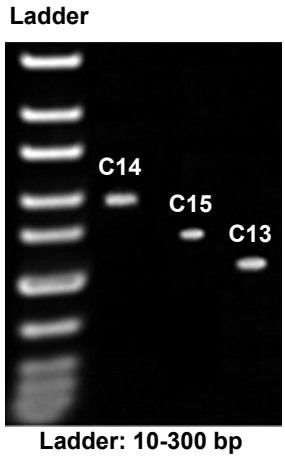

Figure 21. PAGE of **C13-15** SNAs.

3.4.4.2 MS and SEC-MALS analysis of hetero-antennary bioconjugates

The authenticity of the glycoconjugates (**C6-C11**), peptide-glycoconjugate (**C12**) and hexa-armed SNA (**C13**) were verified by MS (ESI-TOF) spectroscopy (**Figure 22A-C,** an example of **C6** (A), **C9** (B) and **C13** (C)). Hexa-armed SNA **C13** produced acceptable m/z data using MS (ESI-TOF) (**Figure 22C**), but the SNA **C14** was not able to produce m/z data using MS (ESI-TOF) and ESI-hybrid quadrupole-orbitrap. Therefore, to determine the molecular weights of **C14** we used SEC-MALS. SNA **C14** resulted in a symmetric major peak (retention time between 7-9 min), that shows 96% mass fraction of the sample (**Figure 22D)**. The MALS was used to evaluate the molecular weight of the main peak, which was near the expected molecular weight (**Table 6**). The obtained molecular masses for **C6-C13** and the SEC-MALS data of **C14** verifies the authenticity of the products.

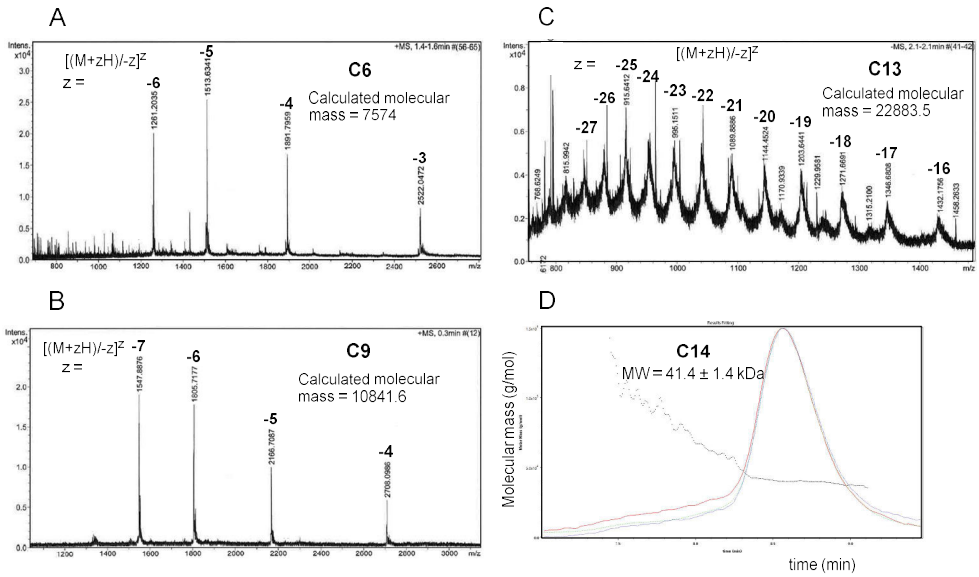

Figure 22. Examples of the MS (ESI-TOF) profile of purified C_{60}-glyco conjugates **C6** (A) and **C9** (B) and **C13** SNA (C). Example of the SEC-MALS profile of purified **C14** SNA (D).

Table 6. Molecular masses of hetero-antennary bioconjugates.

Hetero-antennary bioconjugates	Calculated Molecular Mass /kDa	Observed Molecular Mass /kDa
C6-C8	7.5	7.5[a]
C9-C11	10.8	10.8[a]
C12	13.1	13.1[a]
C13	22.8	22.8[a]
C14	41.4	41.4 ± 1.4[b]

[a] MS (ESI-TOF), [b] SEC-MALS.

3.4.4.3 Atomic force microscopy

Atomic force microscope (AFM) is an excellent tool for identifying nanoparticles and nanomaterials. We used AFM for analysis of **C14** on polyethyleneimine (PEI) coated mica. The monomeric **C14** (**Figure 23**) was represented by particles with a height of around 10 nm. However, the sample also contained bigger and control-sized particles (about 25 nm in height), which might suggest self-assembled aggregates on the PEI-coated mica.

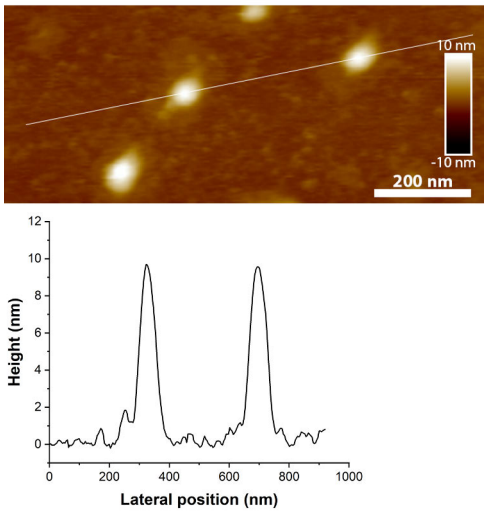

Figure 23. AFM height image of **C14** SNA on PEI-coated mica.

3.4.5 UV melting studies of hetero-antennary **C14** and **C15** SNAs

The hybridization properties of the double helices on the SNAs **C14** and **C15,** and corresponding free duplex (**ON17 + ON18**) were studied by UV melting temperature measurements. Samples **ON17 + ON18** (1.0 µmol) and **C14** and **C15** (2.0 µmol) in 10 mmol L^{-1} sodium cacodylate (pH 7.0) with 0.1 mol L^{-1} NaCl were prepared and the absorbance at 260 nm was recorded over a temperature range of 10-90 °C. **C15** showed 8 °C decreased T_m-value (**Figure 24**) compared to the corresponding free duplex (**ON17 + ON18**). This decreased duplex stability was consistent with earlier results, in which electrostatic and steric repulsion between densely packed oligonucleotides has reported on SNAs [4,110,172–174]. Interestingly, **C14** did not melt at all in the measured temperature range 10-90 °C, referring to a super stable duplex. However, by UV-melting profile analysis we could not yet confirm whether this was just a result of a negligible hyperchromic effect, even if an unwinding of the strands occurs on **C14** (Note: relative hyperchromic effect considered in the melting profiles, **Figure 24**). Further evidence of the super stable duplex could be provided by CD-melting profile analysis below.

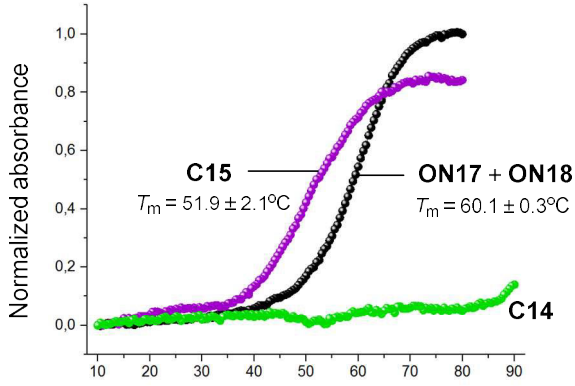

Figure 24. UV Melting profiles of **C14, C15** and **ON17 + ON18** as a control.

3.4.6 CD spectroscopic analysis of hetero-antennary **C14** and **C15** SNAs

Circular dichroism (CD) spectroscopic analysis were used to confirm the helicity variations over the temperature ramp. The measurements were carried out by using SNAs **C14** and **C15** (2.0 µmol) in 10 mmol L^{-1} sodium cacodylate (pH 7.0) with 0.1 mol L^{-1} NaCl. Spectra were recorded from 200 to 400 nm over a temperature range of 10-90 °C. As seen in **Figure 25**, CD profiles of **C15** shown a typical B-type double helix. When the sample temperature increased, the characteristic minimum at 250 nm gradually disappeared because of thermal denaturation. Typical B-type CD-profile can also be seen on **C14**, but what makes this data interesting is that there is no marked difference of the profiles in increasing sample temperature. Even at 90 °C (the bold red line, **Figure 25A**), the profile shows a deep minimum at 250 nm, indicating the presence of B-type double helices. Very stable double helices were known in covalently cross-linked cyclic structures,[190] but **C14** appeared to be an interesting example of dendritic nucleic acids, in which nearby hairpin-type double helices stabilized each other via steric and electrostatic repulsion. Seemingly, there was no space enough for unwinding. Polydisperse gold nanoparticles SNAs with covalently attached RNA double helices has been reported,[174] but no comparable stability phenomena was studied in detail.

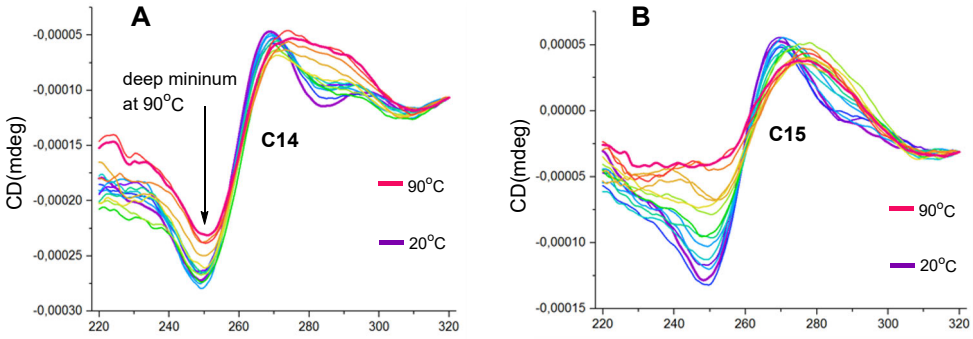

Figure 25. CD profiles of **C14** (A) and **C15** (B) SNAs.

4 Conclusion

A two-step technique for the controlled monofunctionalization of C_{60}-based SNAs (**S1-S6**) has been developed. By using this technique, SNAs can be labelled (DOTA, and Alexa-488 demonstrated) or integrated with other biomolecules (ongoing work with antibodies). The other ON arms of the SNA can be unmodified or may be used to decorate the SNAs outer sphere and this way can affect distribution properties of the SNAs. Appropriate labelling is needed for the monitoring of cellular uptake and biodistribution of molecular SNAs (Alexa 488 and DOTA demonstrated). On the other hand, the label may affect in distribution and cell uptake. Therefore, to minimize the label effect, a developed technique for the controlled monofunctionalization of C_{60}-based SNAs may be useful. We also paid extra attention to homogeneity of the SNAs core units. C_{60}-fullerene core (**1**) was noticed to be readily contaminated by a hardly distinguishable azide-C_{60} [3 + 2] cycloaddition side product (**2**) that would disturb the assembly, purification and identification of the SNAs. The homogeneity and authenticity of the SNAs were determined by RP HPLC, PAGE, CE, DLS, SEC-MALS and MS-ESI spectroscopy. We evaluated the applicability of DOTA as a ^{68}Ga-chelating agent for SNAs. Preliminary radiolabelling studies suggested that the chelation-based techniques should be replaced by a covalent radiolabeling strategy (such as a click reaction with a reactive agent prelabeled with either ^{68}Ga or ^{18}F) to avoid unspecific metal ion (^{68}Ga) binding on the densely packed ON shell of SNAs. This is later confirmed in the laboratories (unpublished results).

Glyco-decorated spherical nucleic acids on a C_{60}-core (**1**) were synthesized and their preliminary cellular uptake with PC3 prostate cancer cells were studied. Nitrone-modified trivalent clusters (**17**, **18α** and **18β**) of carbamoyl mannose and bleomycin disaccharides were prepared and conjugated with an antisense oligonucleotide (**ON8**) via SPANC and the resulting oligonucleotide-conjugates (**ON9-ON11**) were labelled with a fluorescent dye. The labelled glycocluster-oligonucleotide conjugates (**ON12-ON14**) were then hybridized with an SNA (**S6**), and complementary strands, to gain a glycocluster-decorated spherical nucleic acids (**S7-S10**). The formation and stability of the hybridization-mediated SNAs (**S7-S10**)

were evaluated by PAGE, UV melting profile analysis, and time-resolved fluorescence spectroscopy. The cell uptake studies of **ON12-ON15** and corresponding **S7-S10** were tested with PC3 prostate cancer cells. **ONs** with **S6** were taken up by the cells more efficiently than those without **S6**, confirmed by Confocal and Widefield microscopy. A more detailed mechanistic study of internalization and intracellular trafficking is ongoing in the university laboratories. This hybridization-based technique on C_{60}-based SNAs may be an attractive and straightforward technique to emphasize the glyco-cluster effect on the outer sphere of the SNAs, and in this way enhance targeted cell/tissue-specific delivery of ONs.

A bifunctional C_{60}-core (**3**) was synthesized and selectively functionalized by two successive pericyclic click reactions (i.e., iEDDA and SPAAC), in catalyst-free conditions. The applicability of core **3** for a one pot assembly of C_{60}-glycoconjugates (**C9-C11**) and C_{60}-peptide-glycoconjugate (**C12**) has been demonstrated. After the successful synthesis of C_{60}-glycoconjugates, a novel type of SNA (**C14**) with extra ordinary stable covalently bound double helices were prepared by a two-step protocol. Thermal stability of the double helices was verified by UV and CD melting profile experiments. The authenticity and homogeneity of **C9-C12** were verified by RP HPLC, NMR- and MS(ESI-TOF) spectroscopy. The authenticity and homogeneity of **C14** was verified by RP HPLC, PAGE, SEC-MALS and AFM imaging. This strategy allowed synthesis of a variety of hetero-antennary bioconjugates as demonstrated in scheme 9. [142,146,150,185–187] A drug delivery vehicle may need a system that enables loading of tissue/cell-specific ligands and drug payloads in an orthogonal manner, in which the described core **3** may find interesting applications. It may be also useful for assembly of the siRNA loaded SNAs.

5 Experimental

5.1 General methods

All solvents used for synthesis and purification of compounds were reagent grade. Solvents used for air and/or moisture sensitive experiments were dried by using 3 and 4 Å molecular sieves. The synthesis of compounds and their characterizations are described in the original publications. Synthesized compounds were purified by silica gel (230-400 mesh) column chromatography and by RP HPLC when applicable. The novel compounds were characterized by ^{1}H NMR, ^{13}C NMR, 2D NMR, MS-ESI, SEC-MALS, PAGE, DLS, CE and AFM when applicable.

5.2 Oligonucleotide synthesis

The oligonucleotides were synthesized on 1-2 μmol scale on an Applied Biosystems 3400 automated DNA/RNA synthesizer. Commercially available phosphoramidite building blocks and a conventional phosphoramidite coupling cycle were used for oligonucleotides syntheses. Additional information on the syntheses are given in the results and discussion, as well as in the original publications. Oligonucleotides were purified by RP HPLC, by using a semi-preparative Thermo ODS Hypersil C18 (250 × 4.6 mm, 5 μm) column, with a gradient elution from 0 to 100% MeCN in 0.1 mol L^{-1} aqueous triethylammonium acetate over 30 min, flow rate 3.0 mL min^{-1}, UV detection at 260 nm. The authenticity of the purified oligonucleotides was verified by MS (ESI-TOF) spectrometer.

5.3 Peptide synthesis

The amino-modified peptide was synthesized on a 5 μmol scale on a Rink-amide ChemMatrix resin by CEM, Liberty Blue automated peptide synthesizer. Commercially available amino acid building blocks and a conventional amide coupling cycle were used for the peptide synthesis. The peptide was released from the support using a mixture of anisole and trifluoroacetic acid (TFA), precipitated in diethyl ether (Et_2O) and purified by RP HPLC, using a semi-preparative Thermo

ODS Hypersil C18 (250 x 4.6 mm, 5 µm) column, with a gradient elution from 0 to 100% MeCN in 0.1% aqueous TFA over 30 min, flow rate 3.0 mL min^{-1}, UV detection at 280 nm. The authenticity of the purified aminospacer-modified peptide was verified by MS (ESI-TOF) spectrometer. The purified peptide was coupled to commercially available bicyclo [6.1.0]non-4-yn-9-ylmethyl NHS carbonate via standard carbamate-coupling protocol to make BCN-modified peptide. The reaction mixture was purified by RP HPLC, using a semi-preparative Thermo ODS Hypersil C18 (250 x 4.6 mm, 5 µm) column, with a gradient elution from 0 to 100% MeCN in 0.1 mol L^{-1} aqueous triethylammonium acetate over 30 min, flow rate 3.0 mL min^{-1}, UV detection at 280 nm. The authenticity of the purified BCN-modified peptide was verified by MS (ESI-TOF) spectrometer.

5.4 UV melting temperature studies

The UV melting temperatures of ONs and SNAs duplexes were recorded at 260 nm on a Perkin Elmer Lambda 35 UV-visible spectrometer equipped with a Peltier temperature controller unit using quartz cuvettes with 10 mm optical path length. The temperature was changed at a rate of 0.5 °C min^{-1} from 10 to 90 °C for **C14**, whereas 10 to 80 °C for all other samples. Sample concentration for **C14** and **C15** was 2 µmol, whereas 1 µmol for all other samples in 10 mmol L^{-1} sodium cacodylate (pH 7.0) with 0.1 mol L^{-1} NaCl. The melting temperatures of ONs and SNAs duplexes were determined as inflection point of the UV melting curves.

5.5 CD measurements

The CD measurements of oligonucleotide and SNAs duplexes were recorded at 220-320 nm on an Applied Photophysics Chirascan spectrophotometer equipped with a Peltier temperature controller unit. The temperature range of 10 to 90 °C, sampling at 1 °C intervals. Same UV melting studies samples were used for the CD measurements.

Acknowledgements

This thesis is based on experimental work performed in the Laboratory of Organic Chemistry and Chemical Biology at the Department of Chemistry, University of Turku, Finland, during the years of February 2018 to October 2022. The financial support from the Academy of Finland, Business Finland, and Doctoral Programme in Exact Sciences are gratefully acknowledged.

First and foremost, I am deeply grateful to my PhD supervisor Professor Pasi Virta for giving me an opportunity to pursue a doctoral degree under his guidance. I appreciate his immense knowledge and experience in the field of nucleic acid chemistry. I would like to thank you for your continuous encouragement, thoughtful suggestions, support, patience during the years, trust in me, and being a great supervisor. I am also very much grateful to my second PhD supervisor, Associate Professor Tuomas Lönnberg. I want to thank you for your inspiration, support, and valuable advice. In addition, I thank to Dr. Ville Tähtinen for his constant guidance and help.

I extend my gratitude to my collaborators: Professor Anne Roivainen, Ann-Mari Yliperttula, Antti Äärelä, Dr. Ekaterina Lisitsyna, Dr. Elina Vuorimaa-Laukkanen, Dr. Heidi Korhonen, Iida Haapalehto, Dr. Jani Rahkila, Dr. Juan Jose Valle-Delgado, Laura Leimu, Professor Marjo Yliperttula, Professor Monika Österberg, Niko Korsoff, Olli Moisio, Dr. Päivi Poijärvi-Virta, Saara Siekkinen, Dr. Sajal Maity, Dr. Satu Mikkola, Professor Tapani Viitala, Toni Laine, Dr. Victor Nesati and Dr. Ville Tähtinen for their contribution in the papers included in this thesis.

I wish to thank Professor Steven Dowdy and Professor Mikko Oivanen for carefully evaluating my thesis. I am also grateful to Professor Roger Strömberg for accepting to be my opponent.

I want to thank all the people in the Bioorganic Chemistry Group, with whom I have had pleasure to work with during these years: Aapo Aho, Antti Äärelä, Dr. Asmo Aro-Heinilä, Dr. Datta Ukale, Dr. Heidi Korhonen, Lange Saleh, Dr. Madhuri Hande, Mark Afari, Dr. Mikko Ora, Dr. Päivi Poijärvi-Virta, Petteri Lepistö, Dr. Sajal Maity, Dr. Satu Mikkola, Dr. Tharun Kotammagari, Tommi Österlund, Toni Laine, and Dr. Ville Tähtinen. Thank you for your help, advice, great discussions and for providing a pleasant working atmosphere. I would like to thank the

Instrument Centre team: Dr. Alex Dickens, Dr. Jani Rahkila and Dr. Tuomas Karskela for their help with the NMR and MS instruments. I am very grateful to Kari Loikas, Kirsi Laaksonen, Mauri Nauma and Tiina Buss for providing valuable help with chemicals, instruments and IT systems.

I take this opportunity to thank all my friends from *Syngenta Biosciences* for their late-night laughs, parties, advice, outings and many unforgettable memories. Also, I am very much thankful to all my friends in Turku for their friendliness and celebrations: Akash, Ashwini, Joakim, Kedar, Lokesh, Narhari, Plawan, Rahul, Rahul, Rajendra, Renuka, Sachin, Swostik, and Tharun. It has always been fun to see you and to spend time with you.

My special thanks to my grandmother Rukhmini. Unfortunately, you are not in the world to share this milestone, but I am very grateful for your love, care and continuous support throughout my life. You are my daily inspiration to work harder and try more. My sincere thanks to my parents Navnath and Savita. I appreciate your effort and love in bringing me up to be a better individual. Also, I thank my brothers Ajay and Ravindra for their support and everything. Finally, many thanks to Swati for your patience, love, and for all the great times of togetherness.

Turku, October 2022

Vijay Gulumkar

List of References

1. Igarashi J, Niwa Y, Sugiyama D. *Futur Rare Dis*. 2022; 2.
2. Juliano RL. *Nucleic Acids Res*. 2016; 44: 6518–6548.
3. Whitehead KA, Langer R, Anderson DG. *Nat Rev Drug Discov*. 2009; 8: 129–138.
4. Cutler JI, Zhang K, Zheng D, Auyeung E, Prigodich AE, Mirkin CA. *J Am Chem Soc*. 2011; 133: 9254–9257.
5. Mcmahon KM, Foit L, Angeloni NL, Giles FJ, Gordon LI, Thaxton CS. 2015; 166: 129–150.
6. Patel PC, Giljohann DA, Daniel WL, Zheng D, Prigodich AE, Mirkin CA. *Bioconjug Chem*. 2010; 21: 2250–2256.
7. Seferos DS, Prigodich AE, Giljohann DA, Patel PC, Mirkin CA. *Nano Lett*. 2009; 9: 308–311.
8. Massich MD, Giljohann DA, Schmucker AL, Patel PC, Mirkin CA. *ACS Nano*. 2010; 4: 5641–5646.
9. Massich MD, Giljohann DA, Seferos DS, Ludlow LE, Horvath CM, Mirkin CA. *Mol Pharm*. 2009; 6: 1934–1940.
10. Kapadia CH, Melamed JR, Day ES. *BioDrugs*. 2018; 32: 297–309.
11. Jensen SA, Day ES, Ko CH, Hurley LA, Luciano JP, Kouri FM, Merkel TJ, Luthi AC, Patel PC, Cutler JI, Daniel WL, Scott AW, Rotz MW, Meade TJ, Giljohann DA, Mirkin CA, Stegh AH. *Sci Transl Med*. 2013; 5: 1–12.
12. Rosi NL, Giljohann DA, Thaxton CS, Lytton-Jean AKR, Han MS, Mirkin CA. *Science (80-)*. 2006; 312: 1027–1030.
13. Zheng D, Giljohann DA, Chen DL, Massich MD, Wang XQ, Iordanov H, Mirkin CA, Paller AS. *Proc Natl Acad Sci U S A*. 2012; 109: 11975–11980.
14. Giljohann DA, Seferos DS, Prigodich AE, Patel PC, Mirkin CA. *J Am Chem Soc*. 2009; 131: 2072–2073.
15. Calabrese CM, Merkel TJ, Briley WE, Randeria PS, Narayan SP, Rouge JL, Walker DA, Scott AW, Mirkin CA. *Angew Chemie - Int Ed*. 2015; 54: 476–480.
16. Tan X, Lu X, Jia F, Liu X, Sun Y, Logan JK, Zhang K. *J Am Chem Soc*. 2016; 138: 10834–10837.
17. Banga RJ, Krovi SA, Narayan SP, Sprangers AJ, Liu G, Mirkin CA, Nguyen SBT. *Biomacromolecules*. 2017; 18: 483–489.
18. Bousmail D, Amrein L, Fakhoury JJ, Fakih HH, Hsu JCC, Panasci L, Sleiman HF. *Chem Sci*. 2017; 8: 6218–6229.
19. Li S, Jiang Q, Liu Y, Wang W, Yu W, Wang F, Liu X. *Anal Chem*. 2021; 93: 11275–11283.
20. Zhu S, Xing H, Gordiichuk P, Park J, Mirkin CA. *Adv Mater*. 2018; 30: 1–6.
21. Radovic-Moreno AF, Chernyak N, Mader CC, Nallagatla S, Kang RS, Hao L, Walker DA, Halo TL, Merkel TJ, Rische CH, Anantatmula S, Burkhart M, Mirkin CA, Gryaznov SM. *Proc Natl Acad Sci U S A*. 2015; 112: 3892–3897.
22. Stephenson ML, Zamecnik PC. *Proc Natl Acad Sci U S A*. 1978; 75: 285–288.
23. Zamecnik PC, Stephenson ML. *Proc Natl Acad Sci U S A*. 1978; 75: 280–284.
24. Mercuri E, Darras BT, Chiriboga CA, Day JW, Campbell C, Connolly AM, Iannaccone ST, Kirschner J, Kuntz NL, Saito K, Shieh PB, Tulinius M, Mazzone ES, Montes J, Bishop KM, Yang Q, Foster R, Gheuens S, Bennett CF, Farwell W, Schneider E, De Vivo DC, Finkel RS. *N Engl J Med*. 2018; 378: 625–635.

25. Finkel RS, Mercuri E, Darras BT, Connolly AM, Kuntz NL, Kirschner J, Chiriboga CA, Saito K, Servais L, Tizzano E, Topaloglu H, Tulinius M, Montes J, Glanzman AM, Bishop K, Zhong ZJ, Gheuens S, Bennett CF, Schneider E, Farwell W, De Vivo DC. *N Engl J Med*. 2017; 377: 1723–1732.
26. Nyce J. *Curr Opin Allergy Clin Immunol*. 2002; 2: 533–536.
27. Dhuri K, Bechtold C, Quijano E, Pham H, Gupta A, Vikram A, Bahal R. *J Clin Med*. 2020; 9: 1–24.
28. Fire A, Xu S, Montgomery MK, Kostas SA, Driver SE, Mello CC. *Nature*. 1998; 391: 806–811.
29. Mis M, Bernstein E, Caudy AA, Hammond SM, Hannon GJ. *Nature*. 2001; 409: 363–366.
30. Großhans H, Filipowicz W. *Nature*. 2008; 451: 414–416.
31. Kurreck J. *Angew Chemie - Int Ed*. 2009; 48: 1378–1398.
32. Nykänen A, Haley B, Zamore PD. *Cell*. 2001; 107: 309–321.
33. Sibley CR, Seow Y, Wood MJ. *Mol Ther*. 2010; 18: 466–476.
34. Hong CA, Nam YS. *Theranostics*. 2014; 4: 1211–1232.
35. Nakagawa O, Ming X, Huang L, Juliano RL. *J Am Chem Soc*. 2010; 132: 8848–8849.
36. Dohmen C, Fröhlich T, Lächelt U, Röhl I, Vornlocher HP, Hadwiger P, Wagner E. *Mol Ther - Nucleic Acids*. 2012; 1: e7.
37. Willibald J, Harder J, Sparrer K, Conzelmann KK, Carell T. *J Am Chem Soc*. 2012; 134: 12330–12333.
38. Patwa A, Gissot A, Bestel I, Barthélémy P. *Chem Soc Rev*. 2011; 40: 5844–5854.
39. Pokholenko O, Gissot A, Vialet B, Bathany K, Thiéry A, Barthélémy P. *J Mater Chem B*. 2013; 1: 5329–5334.
40. Zhao B, Tian Q, Bagheri Y, You M. *Curr Opin Biomed Eng*. 2020; 13: 76–83.
41. Soutschek J, Akinc A, Bramlage B, Charisse K, Constien R, Donoghue M, Elbashir S, Gelck A, Hadwiger P, Harborth J, John M, Kesavan V, Lavine G, Pandey RK, Racie T, Rajeev KS, Röhl I, Toudjarska I, Wang G, Wuschko S, Bumcrot D, Kotellansky V, Limmer S, Manoharan M, Vornlocher HP. *Nature*. 2004; 432: 173–178.
42. Nagata T, Dwyer CA, Yoshida-Tanaka K, Ihara K, Ohyagi M, Kaburagi H, Miyata H, Ebihara S, Yoshioka K, Ishii T, Miyata K, Miyata K, Powers B, Igari T, Yamamoto S, Arimura N, Hirabayashi H, Uchihara T, Hara RI, Wada T, Bennett CF, Seth PP, Rigo F, Yokota T. *Nat Biotechnol*. 2021; 39: 1529–1536.
43. Nishina K, Unno T, Uno Y, Kubodera T, Kanouchi T, Mizusawa H, Yokota T. *Mol Ther*. 2008; 16: 734–740.
44. Wolfrum C, Shi S, Jayaprakash KN, Jayaraman M, Wang G, Pandey RK, Rajeev KG, Nakayama T, Charrise K, Ndungo EM, Zimmermann T, Koteliansky V, Manoharan M, Stoffel M. *Nat Biotechnol*. 2007; 25: 1149–1157.
45. Biscans A, Coles A, Haraszti R, Echeverria Di, Hassler M, Osborn M, Khvorova A. *Nucleic Acids Res*. 2019; 47: 1082–1096.
46. Osborn MF, Coles AH, Biscans A, Haraszti RA, Roux L, Davis S, Ly S, Echeverria D, Hassler MR, Godinho BMDC, Nikan M, Khvorova A. *Nucleic Acids Res*. 2019; 47: 1070–1081.
47. Varki A. *Glycobiology*. 1993; 3: 97–130.
48. Lis H, Sharon N. *Chem Rev*. 1998; 98: 637–674.
49. Boons GJ, Wu P. *Glycobiology*. 2016; 26: 788.
50. Seeberger PH, Werz DB. *Nature*. 2007; 446: 1046–1051.
51. Ernst B, Magnani JL. *Nat Rev Drug Discov*. 2009; 8: 661–677.
52. Lundquist JJ, Toone EJ. *Chem Rev*. 2002; 102: 555–578.
53. Biessen EAL, Vietsch H, Rump ET, Fluiter K, Kuiper J, Bijsterbosch MK, Van Berkel TJC. *Biochem J*. 1999; 340: 783–792.
54. Nair JK, Willoughby JLS, Chan A, Charisse K, Alam MR, Wang Q, Hoekstra M, Kandasamy P, Kelin A V., Milstein S, Taneja N, Oshea J, Shaikh S, Zhang L, Van Der Sluis RJ, Jung ME, Akinc A, Hutabarat R, Kuchimanchi S, Fitzgerald K, Zimmermann T, Van Berkel TJC, Maier MA, Rajeev KG, Manoharan M. *J Am Chem Soc*. 2014; 136: 16958–16961.
55. Hangeland JJ, Flesher JE, Deamond SF, Lee YC, Ts'o POP, Frost JJ. *Antisense Nucleic Acid Drug Dev*. 1997; 7: 141–149.

56. Duff RJ, Deamond SF, Roby C, Zhou Y, Ts'o POP. *Methods Enzymol*. 2000; 313: 297–321.
57. Biessen BEAL, Vietsch H, Rump ET, Fluiter K. 1999; 314: 324–342.
58. Prakash TP, Graham MJ, Yu J, Carty R, Low A, Chappell A, Schmidt K, Zhao C, Aghajan M, Murray HF, Riney S, Booten SL, Murray SF, Gaus H, Crosby J, Lima WF, Guo S, Monia BP, Swayze EE, Seth PP. *Nucleic Acids Res*. 2014; 42: 8796–8807.
59. Rajeev KG, Nair JK, Jayaraman M, Charisse K, Taneja N, O'Shea J, Willoughby JLS, Yucius K, Nguyen T, Shulga-Morskaya S, Milstein S, Liebow A, Querbes W, Borodovsky A, Fitzgerald K, Maier MA, Manoharan M. *ChemBioChem*. 2015; 16: 903–908.
60. Ugarte-Uribe B, Pérez-Rentero S, Lucas R, Aviñó A, Reina JJ, Alkorta I, Eritja R, Morales JC. *Bioconjug Chem*. 2010; 21: 1280–1287.
61. Reyes-Darias JA, Sánchez-Luque FJ, Morales JC, Pérez-Rentero S, Eritja R, Berzal-Herranz A. *ChemBioChem*. 2015; 16: 584–591.
62. St-Pierre G, Pal S, Østergaard ME, Zhou T, Yu J, Tanowitz M, Seth PP, Hanessian S. *Bioorganic Med Chem*. 2016; 24: 2397–2409.
63. Zhu L, Mahato RI. *Bioconjug Chem*. 2010; 21: 2119–2127.
64. Karskela M, Virta P, Malinen M, Urtti A, Lönnberg H. *Bioconjug Chem*. 2008; 19: 2549–2558.
65. Van Delft P, Meeuwenoord NJ, Hoogendoorn S, Dinkelaar J, Overkleeft HS, Van Der Marel GA, Filippov D V. *Org Lett*. 2010; 12: 5486–5489.
66. Jadhav S, Käkelä M, Mäkilä J, Kiugel M, Liljenbäck H, Virta J, Poijärvi-Virta P, Laitala-Leinonen T, Kytö V, Jalkanen S, Saraste A, Roivainen A, Lönnberg H, Virta P. *Bioconjug Chem*. 2016; 27: 391–403.
67. Sievers EL, Senter PD. *Annu Rev Med*. 2013; 64: 15–29.
68. Uckun FM, Qazi S, Dibirdik I, Myers DE. *Integr Biol (United Kingdom)*. 2013; 5: 122–132.
69. Satake N, Duong C, Yoshida S, Oestergaard M, Chen C, Peralta R, Guo S, Seth PP, Li Y, Beckett L, Chung J, Nolta J, Nitin N, Tuscano JM. *Mol Med*. 2016; 22: 632–642.
70. Arnold AE, Malek-Adamian E, Le PU, Meng A, Martínez-Montero S, Petrecca K, Damha MJ, Shoichet MS. *Mol Ther - Nucleic Acids*. 2018; 11: 518–527.
71. Mullard A. *Nat Rev Drug Discov*. 2022; 21: 6–8.
72. Ellington AD, Szostak JW. *Nature*. 1990; 346: 818–822.
73. White RR, Sullenger BA, Rusconi CP. *J Clin Invest*. 2000; 106: 929–934.
74. McNamara JO, Andrechek ER, Wang Y, Viles KD, Rempel RE, Gilboa E, Sullenger BA, Giangrande PH. *Nat Biotechnol*. 2006; 24: 1005–1015.
75. Lupold SE, Hicke BJ, Lin Y, Coffey DS. *Cancer Res*. 2002; 62: 4029–4033.
76. Dassie JP, Liu XY, Thomas GS, Whitaker RM, Thiel KW, Stockdale KR, Meyerholz DK, McCaffrey AP, McNamara JO, Giangrande PH. *Nat Biotechnol*. 2009; 27: 839–846.
77. Neff CP, Zhou J, Remling L, Kuruvilla J, Zhang J, Li H, Smith DD, Swiderski P, Rossi JJ, Akkina R. *Sci Transl Med*. 2011; 3.
78. Ayatollahi S, Salmasi Z, Hashemi M, Askarian S, Oskuee RK, Abnous K, Ramezani M. *Int J Biochem Cell Biol*. 2017; 92: 210–217.
79. Wang M, Thanou M. *Pharmacol Res*. 2010; 62: 90–99.
80. Kadam RS, Bourne DWA, Kompella UB. *Drug Metab Dispos*. 2012; 40: 1380–1388.
81. Banga RJ, Chernyak N, Narayan SP, Nguyen ST, Mirkin CA. *J Am Chem Soc*. 2014; 136: 9866–9869.
82. Banga RJ, Meckes B, Narayan SP, Sprangers AJ, Nguyen ST, Mirkin CA. *J Am Chem Soc*. 2017; 139: 4278–4281.
83. Mirkin CA, Letsinger RL, Mucic RC, Storhoff JJ. *Nature*. 1996; 382: 607–609.
84. Young KL, Scott AW, Hao L, Mirkin SE, Liu G, Mirkin CA. *Nano Lett*. 2012; 12: 3867–3871.
85. Patil ML, Zhang M, Betigeri S, Taratula O, He H, Minko T. *Bioconjug Chem*. 2008; 19: 1396–1403.
86. Lv Z, Zhu Y, Li F. *Front Bioeng Biotechnol*. 2021; 9.
87. Cutler JI, Auyeung E, Mirkin CA. *J Am Chem Soc*. 2012; 134: 1376–1391.
88. Tapeinos C, Battaglini M, Ciofani G. *J Control Release*. 2017; 264: 306–332.
89. Hoy SM. *Drugs*. 2018; 78: 1625–1631.
90. Lai CC, Shih TP, Ko WC, Tang HJ, Hsueh PR. *Int J Antimicrob Agents*. 2020; 55: 105924.

91. Verbeke R, Lentacker I, De Smedt SC, Dewitte H. *J Control Release*. 2021; 333: 511–520.
92. Hou X, Zaks T, Langer R, Dong Y. *Nat Rev Mater*. 2021; 6: 1078–1094.
93. Zheng S, Wang X, Weng YH, Jin X, Ji JL, Guo L, Hu B, Liu N, Cheng Q, Zhang J, Bai H, Yang T, Xia XH, Zhang HY, Gao S, Huang Y. *Mol Ther - Nucleic Acids*. 2018; 12: 805–816.
94. Kim B, Park JH, Sailor MJ. *Adv Mater*. 2019; 31.
95. Weng Y, Huang Q, Li C, Yang Y, Wang X, Yu J, Huang Y, Liang XJ. *Mol Ther - Nucleic Acids*. 2020; 19: 581–601.
96. Mirkin CA, Letsinger RL, Mucic RC, Storhoff JJ. *Spherical Nucleic Acids*. 2020; 382: 3–11.
97. *Nano Lett 7(7)2112–2115*.
98. Cutler JI, Zheng D, Xu X, Giljohann DA, Mirkin CA. *Nano Lett*. 2010; 10: 1477–1480.
99. Zhang C, MacFarlane RJ, Young KL, Choi CHJ, Hao L, Auyeung E, Liu G, Zhou X, Mirkin CA. *Nat Mater*. 2013; 12: 741–746.
100. Mitchell GP, Mirkin CA, Letsinger RL. *J Am Chem Soc*. 1999; 121: 8122–8123.
101. Li H, Zhang B, Lu X, Tan X, Jia F, Xiao Y, Cheng Z, Li Y, Silva DO, Schrekker HS, Zhang K, Mirkin CA. *Proc Natl Acad Sci U S A*. 2018; 115: 4340–4344.
102. Brodin JD, Auyeung E, Mirkin CA. *Proc Natl Acad Sci U S A*. 2015; 112: 4564–4569.
103. Hao L, Patel PC, Alhasan AH, Giljohann DA, Mirkin CA. *Small*. 2011; 7: 3158–3162.
104. Rouge JL, Hao L, Wu XA, Briley WE, Mirkin CA. *ACS Nano*. 2014; 8: 8837–8843.
105. Seferos DS, Giljohann DA, Rosi NL, Mirkin CA. *ChemBioChem*. 2007; 8: 1230–1232.
106. Patel PC, Giljohann DA, Seferos DS, Mirkin CA. *Proc Natl Acad Sci U S A*. 2008; 105: 17222–17226.
107. Liu B, Wu P, Huang Z, Ma L, Liu J. *J Am Chem Soc*. 2018; 140: 4499–4502.
108. Letsinger RL, Elghanian R, Viswanadham G, Mirkin CA. *Bioconjug Chem*. 2000; 11: 289–291.
109. Meade TJ. Nanotechnology- Based Precision Tools for the Detection and Treatment of Cancer, .
110. Gulumkar V, Äärelä A, Moisio O, Rahkila J, Tähtinen V, Leimu L, Korsoff N, Korhonen H, Poijärvi-Virta P, Mikkola S, Nesati V, Vuorimaa-Laukkanen E, Viitala T, Yliperttula M, Roivainen A, Virta P. *Bioconjug Chem*. 2021; 32: 1130–1138.
111. Sun J, Curry D, Yuan Q, Zhang X, Liang H. *ACS Appl Mater Interfaces*. 2016; 8: 12504–12513.
112. Hurst SJ, Lytton-Jean AKR, Mirkin CA. *Anal Chem*. 2006; 78: 8313–8318.
113. Mokhtarzadeh A, Vahidnezhad H, Youssefian L, Mosafer J, Baradaran B, Uitto J. *Trends Mol Med*. 2019; 25: 1066–1079.
114. Brodin JD, Sprangers AJ, McMillan JR, Mirkin CA. *J Am Chem Soc*. 2015; 137: 14838–14841.
115. Fm K, La H, Wl D, Es D, Hua Y, Hao L, Cy P, Tj M, Ma Q, Ritner C. *Cold Spring Harb Lab Press*. 2015; 2: 25838542.
116. Randeria PS, Seeger MA, Wang XQ, Wilson H, Shipp D, Mirkin CA, Paller AS. *Proc Natl Acad Sci U S A*. 2015; 112: 5573–5578.
117. Lewandowski KT, Thiede R, Guido N, Daniel WL, Kang R, Guerrero-Zayas MI, Seeger MA, Wang XQ, Giljohann DA, Paller AS. *J Invest Dermatol*. 2017; 137: 2027–2030.
118. Sprangers AJ. 2018; 13: 1–14.
119. Melamed JR, Kreuzberger NL, Goyal R, Day ES. *Mol Ther - Nucleic Acids*. 2018; 12: 207–219.
120. Liu H, Kang RS, Bagnowski K, Yu JM, Radecki S, Daniel WL, Anderson BR, Nallagatla S, Schook A, Agarwal R, Giljohann DA, Paller AS. *J Invest Dermatol*. 2020; 140: 435-444.e4.
121. Huang ZN, Callmann CE, Cole LE, Wang S, Mirkin CA. *ACS Nano*. 2021; 15: 13329–13338.
122. Holmes TR, Paller AS. *Pharmaceuticals*. 2020; 13: 1–19.
123. Kumthekar P, Ko CH, Paunesku T, Dixit K, Sonabend AM, Bloch O, Tate M, Schwartz M, Zuckerman L, Lezon R, Lukas R V., Jovanovic B, McCortney K, Colman H, Chen S, Lai B, Antipova O, Deng J, Li L, Tommasini-Ghelfi S, Hurley LA, Unruh D, Sharma N V., Kandpal M, Kouri FM, Davuluri R V., Brat DJ, Muzzio M, Glass M, Vijayakumar V, Heidel J, Giles FJ, Adams AK, James CD, Woloschak GE, Horbinski C, Stegh AH. *Sci Transl Med*. 2021; 13.
124. Tsvetkova D. 2022.
125. Dhar S, Daniel WL, Giljohann DA, Mirkin CA, Lippard SJ. *J Am Chem Soc*. 2009; 131: 14652–14653.
126. Zhang XQ, Xu X, Lam R, Giljohann D, Ho D, Mirkin CA. *ACS Nano*. 2011; 5: 6962–6970.

127. Tan X, Li BB, Lu X, Jia F, Santori C, Menon P, Li H, Zhang B, Zhao JJ, Zhang K. *J Am Chem Soc*. 2015; 137: 6112–6115.
128. Nam J, Thaxton CS, Mirkin CA. *Science (80-)*. 2003; 301: 1884–1887.
129. Nam JM, Stoeva SI, Mirkin CA. *J Am Chem Soc*. 2004; 126: 5932–5933.
130. Georganopoulou DG, Chang L, Nam JM, Thaxton CS, Mufson EJ, Klein WL, Mirkin CA. *Proc Natl Acad Sci U S A*. 2005; 102: 2273–2276.
131. Thaxton CS, Elghanian R, Thomas AD, Stoeva SI, Lee JS, Smith ND, Schaeffer AJ, Klocker H, Horninger W, Bartsch G, Mirkin CA. *Proc Natl Acad Sci U S A*. 2009; 106: 18437–18442.
132. Prigodich AE, Randeria PS, Briley WE, Kim NJ, Daniel WL, Giljohann DA, Mirkin CA. *Anal Chem*. 2012; 84: 2062–2066.
133. Liu B, Liu J. *J Am Chem Soc*. 2017; 139: 9471–9474.
134. Yeo DC, Wiraja C, Paller AS, Mirkin CA, Xu C. *Nat Biomed Eng*. 2018; 2: 227–238.
135. Yan R, Chen J, Wang J, Rao J, Du X, Liu Y, Zhang L, Qiu L, Liu B, Zhao Y Di, Jiang P, Chen C, Li YQ. *Small*. 2018; 14: 1–12.
136. Lin M, Yi X, Huang F, Ma X, Zuo X, Xia F. *Anal Chem*. 2019; 91: 2021–2027.
137. Kroto HW, Heath JR, O'Brien SC, Curl RF, Smalley RE. *Nature*. 1985; 318: 162–163.
138. Yan W, Seifermann SM, Pierrat P, Bräse S. *Org Biomol Chem*. 2015; 13: 25–54.
139. Zhai WQ, Jiang SP, Peng RF, Jin B, Wang GW. *Org Lett*. 2015; 17: 1862–1865.
140. Vidal S. *Nat Chem*. 2016; 8: 4–6.
141. Liu GF, Filipović M, Ivanović-Burmazović I, Beuerle F, Witte P, Hirsch A. *Angew Chemie - Int Ed*. 2008; 47: 3991–3994.
142. Nierengarten I, Nierengarten JF. *Chem - An Asian J*. 2014; 9: 1436–1444.
143. Lamparth I, Maichle-Mössmer C, Hirsch A. *Angew Chem Int Ed*. 1995; 34: 1607–1609.
144. Li H, Haque SA, Kitaygorodskiy A, Meziani MJ, Torres-Castillo M, Sun YP. *Org Lett*. 2006; 8: 5641–5643.
145. Iehl J, Pereira De Freitas R, Delavaux-Nicot B, Nierengarten JF. *Chem Commun*. 2008; 7345: 2450–2452.
146. Articles F. *Chem Commun*. 2010; 46: 1–5.
147. Lehl J, Nierengarten JF. *Chem - A Eur J*. 2009; 15: 7306–7309.
148. Fortgang P, Maisonhaute E, Amatore C, Delavaux-Nicot B, Iehl J, Nierengarten J-F. *Angew Chemie*. 2011; 123: 2412–2415.
149. Iehl J, Nierengarten JF, Harriman A, Bura T, Ziessel R. *J Am Chem Soc*. 2012; 134: 988–998.
150. Muñoz A, Sigwalt D, Illescas BM, Luczkowiak J, Rodríguez-Pérez L, Nierengarten I, Holler M, Remy JS, Buffet K, Vincent SP, Rojo J, Delgado R, Nierengarten JF, Martín N. *Nat Chem*. 2016; 8: 50–57.
151. Abellán Flos M, García Moreno MI, Ortiz Mellet C, García Fernández JM, Nierengarten JF, Vincent SP. *Chem - A Eur J*. 2016; 22: 11450–11460.
152. Trinh TMN, Holler M, Schneider JP, García-Moreno MI, García Fernández JM, Bodlenner A, Compain P, Ortiz Mellet C, Nierengarten JF. *J Mater Chem B*. 2017; 5: 6546–6556.
153. Ramos-Soriano J, Reina JJ, Pérez-Sánchez A, Illescas BM, Rojo J, Martín N. *Chem Commun*. 2016; 52: 10544–10546.
154. Ramos-Soriano J, Reina JJ, Illescas BM, Rojo J, Martín N. *J Org Chem*. 2018; 83: 1727–1736.
155. Meichsner E, Schillinger F, Trinh TMN, Guerra S, Hahn U, Nierengarten I, Holler M, Nierengarten JF. *European J Org Chem*. 2021; 2021: 3787–3797.
156. Li H, Li Y, Xiao Y, Zhang B, Cheng Z, Shi J, Xiong J, Li Z, Zhang K. *Bioconjug Chem*. 2020; 31: 530–536.
157. Grösser T, Prato M, Lucchini V, Hirsch A, Wudl F. *Angew Chemie Int Ed English*. 1995; 34: 1343–1345.
158. Prato M, Li QC, Wudl F, Lucchini V. *J Am Chem Soc*. 1993; 115: 1148–1150.
159. Cases M, Duran M, Mestres J, Martín N, Solà M. *J Org Chem*. 2001; 66: 433–442.
160. Iehl J, Nierengarten JF. *Chem Commun*. 2010; 46: 4160–4162.
161. Kiviniemi A, Mäkelä J, Mäkilä J, Saanijoki T, Liljenbäck H, Poijärvi-Virta P, Lönnberg H, Laitala-Leinonen T, Roivainen A, Virta P. *Bioconjug Chem*. 2012; 23: 1981–1988.

162. Österlund T, Aho A, Äärelä A, Tähtinen V, Korhonen H, Virta P. *Curr Protoc Nucleic Acid Chem*. 2020; 83.
163. Luna Velez M V., Verhaegh GW, Smit F, Sedelaar JPM, Schalken JA. *Oncogene*. 2019; 38: 3696–3709.
164. An F, Gong B, Wang H, Yu D, Zhao G, Lin L, Tang W, Yu H, Bao S, Xie Q. *Apoptosis*. 2012; 17: 702–716.
165. Guo CJ, Pan Q, Li DG, Sun H, Liu BW. *J Hepatol*. 2009; 50: 766–778.
166. Mäkilä J, Jadhav S, Kiviniemi A, Käkelä M, Liljenbäck H, Poijärvi-Virta P, Laitala-Leinonen T, Lönnberg H, Roivainen A, Virta P. *Bioorganic Med Chem*. 2014; 22: 6806–6813.
167. Mäkilä J, Kiviniemi A, Saanijoki T, Liljenbäck H, Käkelä M, Jadhav S, Poijärvi-Virta P, Lönnberg H, Laitala-Leinonen T, Virta P, Roivainen A. *Mol Pharm*. 2019; 16: 1507–1515.
168. Vanderwielen B, Sharp J, Mobley C, Schaefer K, Pratt C. .
169. Taton TA, Mirkin CA, Letsinger RL. *Science (80-)*. 2000; 289: 1757–1760.
170. Storhoff JJ, Lazarides AA, Mucic RC, Mirkin CA, Letsinger RL, Schatz GC. *J Am Chem Soc*. 2000; 122: 4640–4650.
171. Jin R, Wu G, Li Z, Mirkin CA, Schatz GC. *J Am Chem Soc*. 2003; 125: 1643–1654.
172. Randeria PS, Jones MR, Kohlstedt KL, Banga RJ, Olvera De La Cruz M, Schatz GC, Mirkin CA. *J Am Chem Soc*. 2015; 137: 3486–3489.
173. Fong LK, Wang Z, Schatz GC, Luijten E, Mirkin CA. *J Am Chem Soc*. 2018; 140: 6226–6230.
174. Yamankurt G, Stawicki RJ, Posadas DM, Nguyen JQ, Carthew RW, Mirkin CA. *Proc Natl Acad Sci U S A*. 2020; 117: 1312–1320.
175. Keinänen O, Fung K, Pourat J, Jallinoja V, Vivier D, Pillarsetty NVK, Airaksinen AJ, Lewis JS, Zeglis BM, Sarparanta M. *EJNMMI Res*. 2017; 7.
176. Mushtaq S, Yun SJ, Jeon J. *Molecules*. 2019; 24.
177. Tekie FSM, Hajiramezanali M, Geramifar P, Raoufi M, Dinarvand R, Soleimani M, Atyabi F. *Sci Rep*. 2020; 10: 9664.
178. Chinen AB, Guan CM, Ko CH, Mirkin CA. *Small*. 2017; 13: 1–8.
179. Yu Z, Schmaltz RM, Bozeman TC, Paul R, Rishel MJ, Tsosie KS, Hecht SM. *J Am Chem Soc*. 2013; 135: 2883–2886.
180. Bhattacharya C, Yu Z, Rishel MJ, Hecht SM. *Biochemistry*. 2014; 53: 3264–3266.
181. Yu Z, Paul R, Bhattacharya C, Bozeman TC, Rishel MJ, Hecht SM. *Biochemistry*. 2015; 54: 3100–3109.
182. Maity SK, Yim C Bin, Jadhav S, Verhassel A, Tuomela J, Solin O, Grönroos TJ, Virta P. *European J Org Chem*. 2019; 2019: 156–163.
183. Boger DL, Honda T. *J Am Chem Soc*. 1994; 116: 5647–5656.
184. MacKenzie DA, Sherratt AR, Chigrinova M, Cheung LLW, Pezacki JP. *Curr Opin Chem Biol*. 2014; 21: 81–88.
185. Cecioni S, Oerthel V, Iehl J, Holler M, Goyard D, Praly JP, Imberty A, Nierengarten JF, Vidal S. *Chem - A Eur J*. 2011; 17: 3252–3261.
186. Durka M, Buffet K, Iehl J, Holler M, Nierengarten JF, Taganna J, Bouckaert J, Vincent SP. *Chem Commun*. 2011; 47: 1321–1323.
187. Compain P, Decroocq C, Iehl J, Holler M, Hazelard D, Barragán TM, Mellet CO, Nierengarten JF. *Angew Chemie - Int Ed*. 2010; 49: 5753–5756.
188. Virta P, Karskela M, Lönnberg H. *J Org Chem*. 2006; 71: 1989–1999.
189. Lönn P, Kacsinta AD, Cui XS, Hamil AS, Kaulich M, Gogoi K, Dowdy SF. *Sci Rep*. 2016; 6: 1–9.
190. El-Sagheer AH, Kumar R, Findlow S, Werner JM, Lane AN, Brown T. *ChemBioChem*. 2008; 9: 50–52.

TURUN
YLIOPISTO
UNIVERSITY
OF TURKU

Painosalama Oy, Turku, Finland 2022

ISBN 978-951-29-9025-2 (PRINT)
ISBN 978-951-29-9026-9 (PDF)
ISSN 0082-7002 (Print)
ISSN 2343-3175 (Online)